Imaging Myocardial Metabolism

11

Robert J. Gropler and Craig R. Malloy

Abbreviations

ATP	Adenosine triphosphate
DNP	Dynamic nuclear polarization
HP	Hyperpolarization
LV	Left ventricle
MRI	Magnetic resonance imaging
MRS	Magnetic resonance spectroscopy
PDH	Pyruvate dehydrogenase
PET	Positron emission computed tomography
PPP	Pentose phosphate pathway
RV	Right ventricle
SPECT	Single photon emission computed tomography
TCA	Tricarboxylic acid
TG	Triglycerides

R.J. Gropler (✉)
Division of Radiological Sciences, Mallinckrodt Institute of Radiology, Washington University School of Medicine, St. Louis, MO, USA
e-mail: groplerr@mir.wustl.edu

C.R. Malloy
Departments of Radiology and Internal Medicine, Advanced Imaging Research Center, University of Texas Southwestern Medical Center, Dallas, TX, USA

VA North Texas Health Care System, Dallas, TX, USA
e-mail: craig.malloy@utsouthwestern.edu

11.1 Introduction

Metabolism of exogenous and endogenous substrates, under baseline conditions and in response to metabolic and physiological stimuli, is central to cardiac myocyte health. The ever-burgeoning body of evidence demonstrating the primacy of perturbations in intermediary metabolism in the pathogenesis of common cardiovascular diseases such as ischemic heart disease, heart failure, and diabetic cardiomyopathy further supports this contention. It is becoming increasingly apparent that chronic adaptations in cellular metabolism initiate a host of pleiotropic actions detrimental to cellular health such as impaired energetics, increases in inflammation, oxidative stress, and apoptosis. Indeed the importance of altered intermediary metabolism underlying human cardiovascular disease is exemplified by the robust drug discovery and development efforts to identify new metabolic modulators.

Radionuclide imaging by positron emission tomography (PET) and single photon emission computed tomography (SPECT) are the most powerful used methods to perform in vivo assessments of myocardial metabolism. PET is currently the gold standard for imaging myocardial metabolism in humans. Its high sensitivity, resulting in the administration of nano- to picomolar concentrations of various radiotracers, and inherent quantitative capability permit the measurement of fluxes in

J.S. Lewis, K.R. Keshari (eds.), *Imaging and Metabolism*, DOI 10.1007/978-3-319-61401-4_11

absolute rates through key metabolic processes without perturbing the biochemical system. SPECT can also measure myocardial metabolism under baseline conditions but is nonquantitative and lacks the availability of an extensive portfolio of metabolic radiotracers. Both methods suffer from the inability to simultaneously measure multiple metabolic processes which is certainly desirable given the complexity of cellular metabolism in health and disease.

Nuclear magnetic resonance (NMR) spectroscopy and imaging methods are valuable tools, but their use in humans is practically impossible due to the combination of the low concentration of the relevant metabolites plus low NMR sensitivity of these nuclei with a detection threshold of millimolar concentrations. Hyperpolarization produces a temporary redistribution of nuclear spin populations and partially overcomes this sensitivity limitation while preserving the chemical specificity inherent in NMR. This technology was well known within the physics community for decades, but it was not until Ardenkjaer-Larsen, Golman, and colleagues demonstrated that the hyperpolarized state could be achieved temporarily under physiologically relevant conditions that potential in vivo assessments could be realized [1, 2]. Since this technology is applicable at conventional MR fields, it is possible to utilize standard MR scanners, coils, and other technologies, which are safe for humans [3]. There is considerable interest in developing hyperpolarized MR-based contrast agents for cardiac studies in humans. From a metabolic perspective, specific substrates labeled with ^{13}C offer the potential to simultaneously assess diverse metabolic pathways. However, MR imaging of hyperpolarized ^{13}C (^{13}C-HP) does present significant challenges for routine imaging such as the significant time constraints due to a short T_1. Furthermore, due to the administration of millimolar concentrations of material, metabolic conditions are perturbed which complicates the interpretation of the measurements.

This first portion of this chapter will summarize the fundamentals of myocardial metabolism and important regulatory mechanisms, highlighting aspects that are relevant to design and interpretation of PET or ^{13}C-HP studies. Although intermediary metabolism, energy capture, and biosynthetic pathways in the heart are complex, the key features can be understood as interacting modules and pathways. The second portion will detail the relative strengths and weaknesses of radionuclide imaging focusing on PET and ^{13}C-HP to assess myocardial metabolism. Compared to hyperpolarization methods, clinical radionuclide methods are far more mature. There is no experience with hyperpolarization methods in heart disease in humans. PET and ^{13}C-HP may be able to provide complementary information on myocardial metabolism. Accordingly, the final portion of the chapter will briefly discuss the metabolic perturbations associated with some common cardiovascular diseases and present potential scenarios whereby synergies may be realized by combining these two technologies.

11.2 Energy Production and Related Metabolic Pathways

Every metabolic pathway is complex, and control mechanisms operate at the level of enzyme expression, the interactions with cofactors, and the concentrations of substrates and products in the local environment. A useful generalization is to separate heart metabolism into distinct modules such as the citric acid cycle, glycolysis, the pentose phosphate pathway, and β-oxidation linked by a few key molecules at metabolic crossroads. These critical molecules are acetyl-CoA (the final common product of multiple pathways), pyruvate (linking the product of glycolysis with exogenous pyruvate and lactate), and glucose-6-phosphate (linking glycolysis, glycogenolysis, and the pentose phosphate pathway). This section presents a brief overview of helpful concepts for understanding the design and interpretation of studies with tracers in the heart. It will also serve to point out important aspects of cardiac metabolism that are currently difficult to probe. The focus is on key metabolites at metabolic

crossroads since these molecules or their analogues are targeted in metabolic imaging.

The vast majority of the energy driving cardiac function comes from the oxidation of acetyl-CoA in the citric acid cycle. The heart normally generates acetyl-CoA from a complex mixture of exogenous substrates including fatty acids of various chain lengths, glucose, lactate, pyruvate and the ketones, acetoacetate, and β-hydroxybutyrate (Fig. 11.1). The relative concentrations may vary dramatically under both physiological and pathological conditions. Studies of isolated hearts in which only a single substrate or perhaps two substrates are supplied do not reflect the pattern of energy production observed in vivo. In general, the heart readily switches among substrates to generate acetyl-CoA [4, 5]. If glucose is the only substrate available to the heart, it is readily oxidized to acetyl-CoA, but the contribution of glucose to acetyl-CoA is negligible when a physiological mixture of substrates is available [6, 7]. Under normal conditions of perfusion and oxygen tension, the majority of energy production in the heart is derived from oxidation of long-chain fatty acids. A significant contribution is also derived from ketones and lactate [6, 7]. During a fast, the contribution of ketones to energy production increases substantially, and the contribution of lactate may increase markedly during exercise [8]. Under abnormal conditions, for example, left

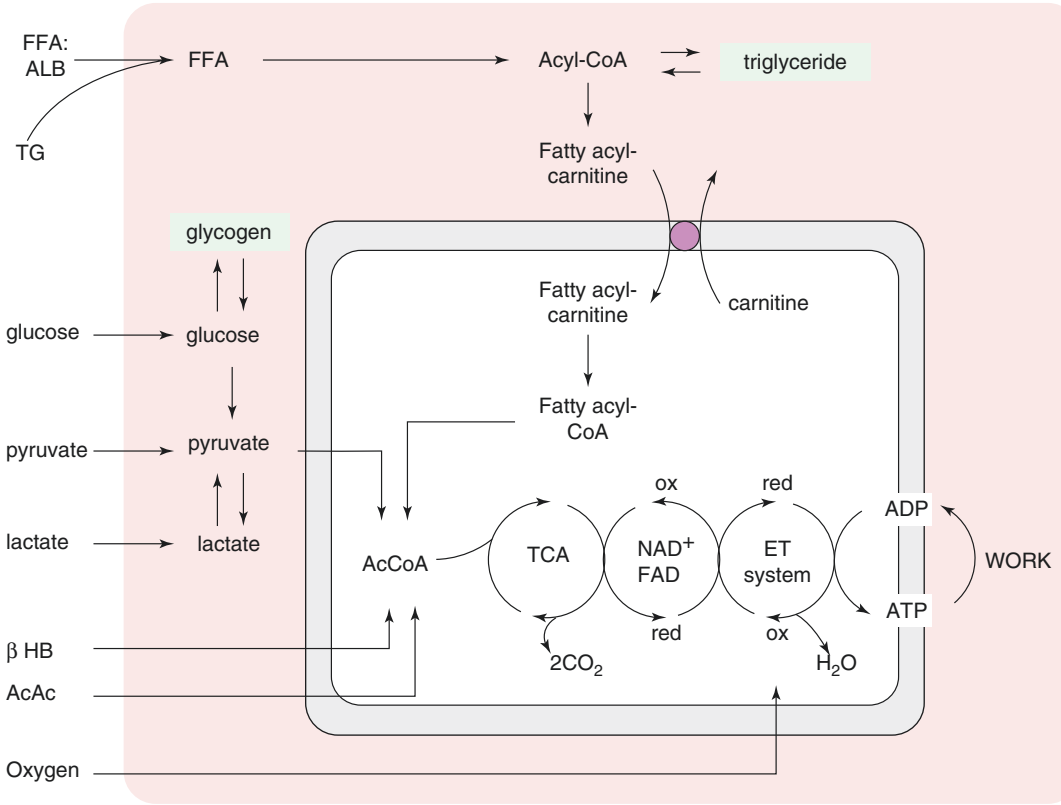

Fig. 11.1 Processes for energy capture in the heart. The heart in vivo is provided with a complex mixture of substrates including long-chain fatty acids, glucose, ketones, lactate, and pyruvate in varying combinations. The normal heart rapidly shifts among these available substrates as well as the stored energy sources, triglycerides, and glycogen, depending on the concentrations of substrates, the presence of insulin and other hormones, and the workload. *AcAc* acetoacetate, *βHB* β-hydroxybutyrate, *ET* electron transport, *FFA* free fatty acids

ventricular (LV) pressure-overload hypertrophy, oxidation of glucose increases substantially. Consequently, one of the challenges of understanding cardiac energy metabolism is that it is governed by at least three factors – plasma substrate concentration, normal physiological responses to energy demands, and disease.

11.2.1 Acetyl-CoA from β-Oxidation of Ketones and Fatty Acids

The concentration of fatty acids in plasma strongly influences the rate of uptake by the heart. The normal range of free fatty acids is roughly 0.2–0.8 mM but can reach 1.0 mM due to stress or conditions such as diabetes or starvation. Actually, long-chain fatty acids are water insoluble and therefore are always bound to albumin or incorporated into triglyceride (TG), either as chylomicrons or very low-density lipoproteins. After transport across the sarcolemma, a long-chain fatty acid is transiently bound to a fatty acid binding protein and subsequently activated by fatty acyl-CoA synthase. The product of this reaction, long-chain fatty acyl-CoA, may either be esterified to TG by glycerophosphate acyltransferase or converted to long-chain fatty acylcarnitine by carnitine palmitoyltransferase (Fig. 11.1). The fate of a fatty acid – esterification and storage vs. oxidation – is a critical branch point in metabolism of long-chain fatty acids. About 80% of radiolabeled oleate or palmitate is rapidly metabolized via ß-oxidation and the citric acid cycle. This suggests that about 20% of fatty acids entering a cardiomyocyte must enter the intracardiac TGTCA pool. However recent observations suggest preferential oxidation of fatty acids may occur via continuous mixing and cycling within the TG pool, suggesting the preferential route for fatty acid oxidation is still an open question [9]. It is important to be aware that cardiomyocytes may store TGs because these fatty acids can be mobilized during adrenergic stimulation and may provide a source of fatty acids for oxidation [10].

As noted above, the majority of long-chain fatty acids are oxidized for energy production. The cytoplasmic long-chain fatty acyl-CoA cannot penetrate the inner mitochondrial membrane and for this reason is converted to a fatty acyl carnitine, described above, by carnitine palmitoyl transferase I (CPT-1). Carnitine acyltranslocase transports this long-chain acylcarnitine across the inner mitochondrial membrane. Finally, the long-chain acyl-CoA is regenerated in the mitochondrial matrix by CPT-2. Within the mitochondria, fatty acids undergo repeated cycles of ß-oxidation to generate acetyl-CoA for oxidation in the citric acid cycle.

[1-^{11}C]acetate has been studied [11] as a tracer for the assessment of citric acid cycle flux in the myocardium. The time-activity curve of ^{11}C may be interpreted in terms of the tricarboxylic acid cycle (TCA) flux and oxygen consumption. Unlike long-chain fatty acids, acetate may be oxidized without the need for the carnitine palmitoyl transferase (CPT) system to cross the inner mitochondrial membrane. In addition to oxidation in the TCA cycle, acetate also participates in an important energy-buffering system in the myocardium catalyzed by carnitine acetyltransferse. This enzyme, located in the mitochondria, interconverts acetyl-CoA with acetylcarnitine [12, 13, 21]. Consequently, the excess concentration of acetyl groups, whether derived from infused acetate, carbohydrates, or fatty acids, can be buffered.

β-Hydroxybutyrate and acetoacetate are ketones that arise from metabolism of fatty acids in the liver. Like fatty acids, the heart oxidizes ketones at a rate dependent on the concentration in plasma. Consequently, the contribution of ketones to acetyl-CoA can shift dramatically depending on nutritional and neurohumoral conditions. The concentration of ketones is normally low in a fed, rested mammal, in the range of 0.03–0.06 millimolar [14, 15]. Considering the low concentration of ketones normally present in plasma, approximately 10x lower than fatty acids, it is perhaps surprising that ketones contribute to energy production at all [6]. During starvation, heart failure, or poorly managed type 1 diabetes, the concentrations can rise dramatically into the millimolar range and markedly suppress oxidation of both fatty acids and carbohydrates. Hence, under these conditions ketones may provide essentially all acetyl-CoA in the myocardium. For this reason it is important to be aware of the nutritional conditions when interpreting metabolic imaging studies.

11.2.2 Pyruvate and Lactate

Pyruvate is a substrate for pyruvate dehydrogenase (PDH), a regulatory site in cellular metabolism that links the TCA cycle and subsequent oxidative phosphorylation with key steps in glucose, lipid, and amino acid metabolism. Pyruvate levels in the blood are typically low (normally ~0.1 mM). Under normal physiological conditions, intracellular pyruvate is readily produced by conversion from lactate. However, after bolus administration, the heart rapidly oxidizes pyruvate. Like the concentration of ketones, the concentration of lactate (normally 1.0–1.2 mM) may vary substantially depending on the physiological response to exercise or disease. The heart is normally a net consumer of lactate, although during ischemia it may actually produce lactate. The enzyme interconverting lactate and pyruvate, lactate dehydrogenase, is highly active in the myocardium, so the heart readily metabolizes lactate (after conversion to pyruvate) when the plasma concentration rises. Pyruvate has four fates in the heart: decarboxylation to form acetyl-CoA for subsequent oxidation in the citric acid cycle, transamination to alanine, reduction to lactate, and carboxylation to form oxaloacetate.

Decarboxylation by PDH is irreversible, and this reaction plays a key role in regulating fatty acid and carbohydrate oxidation. PDH is located in the mitochondrial matrix and flux is regulated by both covalent modification and feedback inhibition [16]. Interestingly, certain fatty acids may paradoxically stimulate PDH [17, 18]. The cycle of covalent modification, phosphorylation-dephosphorylation, is controlled by PDH kinase and PDH phosphatase, respectively. High concentrations of pyruvate favor flux through PDH which is consistent with inhibition of the kinase (less phosphorylation of PDH). Flux through PDH is also stimulated by a low [acetyl-CoA]/[free CoA] and a low NADH/NAD^+ ratio. In the heart, the dominant isoform of PDH kinase is PDH kinase 4; its expression is induced by diabetes, starvation, and peroxisome proliferator activator receptor ligands. Under all these conditions, PDH phosphorylation is expected to increase, thereby inhibiting oxidation of pyruvate or upstream carbohydrates. Under starvation conditions, this effect is teleologically appropriate since it would have the effect of preserving carbohydrates for brain metabolism. Dephosphorylation of PDH (activation of PDH) by the phosphatase is increased by calcium, which in turn is sensitive to adrenergic stimulation or other interventions that drive increased [Ca^{++}] in the mitochondria and are associated with increased myocardial contractility.

Carboxylation of pyruvate to form oxaloacetate is quantitatively a minor pathway in pyruvate metabolism compared to potential flux through PDH [19–21]. Nevertheless, this pathway is likely important in understanding cardiac metabolism. The sum of TCA cycle intermediates varies substantially depending on available substrates and work state. Since the concentration of citrate may play a role in regulation of glycolysis, the total mass of TCA cycle intermediates may influence glucose metabolism. The myocardium has the capacity to remodel and hypertrophy; thus, metabolic pathways necessary for biosynthetic and degradation reactions involving amino acids are likely important. However, no imaging method is available to directly assess this reaction in vivo.

In addition to these two reactions in the mitochondria, decarboxylation to acetyl-CoA and carboxylation to oxaloacetate, pyruvate may also undergo exchange reactions in the cytosol. Transamination to alanine is catalyzed by alanine aminotransferase in the overall reaction: pyruvate + glutamate → alanine + α-ketoglutarate. Pyruvate may also be reduced to lactate by lactate dehydrogenase, a reaction requiring NADH as a cofactor. Consequently the rate of conversion of pyruvate to lactate (but not alanine) should be sensitive to redox conditions.

11.2.3 Glucose and Glycogen

Glucose and glycogen are mentioned last because at physiological concentrations of fatty acids, ketones, and lactate, both substrates contribute little to the overall energy production in the healthy, well-oxygenated myocardium. Nevertheless, glucose metabolism plays an important role in myocardial energetics, for a number of reasons. First, glycolysis and glycogenolysis provide energy buffers during periods

of stress and protect the myocardium during periods of brief ischemia. Second, the pentose phosphate pathway (PPP) is an important source of NADPH which is required for protection of the myocardium from oxidative stress. Third, adenosine triphosphate (ATP) derived from glycolysis may preferentially drive membrane bound ion pumps.

Transport of glucose across the sarcolemma is sensitive to the concentration of extracellular glucose and the activity of glucose transporters in the cell membrane. The main transporter, GLUT-4, is translocated from intracellular vesicles to the membrane in response to ischemia, insulin, increased work load, or activation of AMP-activated protein kinase. The net effect is to increase the availability of intracellular glucose during periods of hyperglycemia or myocardial stress. Once glucose enters the cytosol, it is rapidly phosphorylated, effectively trapping the carbon skeleton in the cytosol because the highly charged phosphate group prevents diffusion or transport out of the cardiomyocyte. Another source of glucose-6-phosphate is degradation of glycogen. Glycogenolysis is stimulated in the heart by increases in cAMP (due to adrenergic stimulation or glucagon), increases in [Ca^{++}], increased [inorganic phosphate], or reduced ATP.

The overall regulation of glycolysis has been intensively investigated and reviewed in detail [22]. Two sites of regulation may be mentioned briefly. First, phosphofructokinase-1 (PFK-1) uses ATP to convert fructose-1-phosphate to fructose 1,6-bisphosphate. This reaction is activated by adenosine diphosphate, adenosine monophosphate, and inorganic phosphate (ADP, AMP, and Pi). Consequently, during periods of myocardial stress (defined by an increased concentration of ATP breakdown products), the reaction is accelerated. Citrate is a negative regulator of PFK-1, and Philip Randle initially proposed that accumulation of citrate due to fatty acid oxidation may inhibit glycolysis, thus linking mitochondrial metabolism to glycolysis at an early step. A second important component in regulation of glycolysis is glyceraldehyde-3-phosphate dehydrogenase (GAPDH). Glyceraldehyde 3-phosphate is converted to 1,3-diphosphoglycerate and in the process generates the NADH produced in glycolysis. A high concentration of NADH in the cytosol will inhibit glycolysis at this step, as is the case during ischemia. Glycolysis is inhibited by accumulation of NADH unless NAD^+ can be regenerated by conversion of pyruvate to lactate and export of lactate.

Other than the generation of pyruvate and energy, glucose metabolism may be important for other processes. Glucose-6-phosphate is the substrate for the PPP (also termed the hexose monophosphate shunt or the phosphogluconate pathway). The PPP has two functions: the generation of NADPH, which is used in virtually all biosynthetic pathways and also reduces oxidized glutathione, and the generation of pentoses which are necessary for nucleotide synthesis. Since these are essential cellular processes, it seems likely that the PPP is important in the heart [23–25]. However, no imaging method is available to specifically probe the PPP.

11.2.4 Anaplerosis

Anaplerosis refers to any reaction that provides a net addition of a carbon skeleton to the TCA cycle [21, 26] . This is in contrast to the oxidation of acetyl-CoA in which two carbons are added to the TCA cycle with release of two molecules of CO_2 per cycle. Anaplerosis is required to maintain the concentration of TCA cycle intermediates which may be lost at a slow rate during biosynthetic reactions or leakage of intermediates from the cardiomyocyte. Pyruvate carboxylation is probably the most important pathway for anaplerosis with carboxylation of propionate, an odd-carbon fatty acid, being a lesser contributor [21, 27, 28]. Flux through pyruvate carboxylase is low, roughly 5–10% of TCA flux [29]. Although most metabolic imaging research has focused on oxidative pathways, it is likely that methods to specifically detect propionate or pyruvate carboxylation will be relevant in understanding cardiac remodeling disorders.

11.2.5 Compartmentation of Pyruvate Metabolism

There is strong evidence from tracer studies with exogenous pyruvate, lactate, and glucose that intracellular pyruvate cannot be treated as one fully mixed pool, even under steady-state conditions [30]. Years ago, Hassinen and colleagues reported that there are two intracellular pools of pyruvate, a pool derived from glycolysis and a peripheral pool that communicates with extracellular pyruvate, intracellular alanine, and intramitochondrial pyruvate [27]. These results were confirmed by others using the radiotracer technique [31, 32] that demonstrated some intracellular pyruvate is inaccessible to extracellular lactate. The production ratio of [^{14}C]bicarbonate relative to [1-^{14}C]lactate activity after administration of [1-^{14}C]]pyruvate was sensitive to the presence of glucose and was interpreted as evidence for multiple kinetically distinct pools of pyruvate in the heart [19]. Furthermore, acetyl-CoA derived from pyruvate originating from glucose is channeled preferentially to acetylcarnitine compared to acetyl-CoA [33].

^{13}C NMR isotopomer studies also found evidence for intracellular compartmentalization of glycolytic and glycogenolytic enzymes in isolated rat hearts perfused with [1-^{13}C]glucose [34]. Studies with [1-^{13}C]glucose [30] found that alanine and acetyl-CoA enrichments were similar under steady-state conditions, but the enrichment in intracellular lactate was less than alanine [35]. These observations strongly suggest that rapid exchange of extracellular labeled pyruvate and lactate with all intracellular pools is not consistent with experimental results. Hyperpolarization has the potential to monitor evolution of labeled lactate and bicarbonate from enriched pyruvate with high temporal resolution, offering the opportunity to probe subcellular compartments and examine the kinetic flexibility of the heart in response to stress and physiological stimuli.

11.3 Radionuclide Methods to Image Metabolism

Imaging of myocardial metabolism using radionuclides is widely applied in cardiovascular investigation as well as the clinical management of the cardiac patient. Detection of viable myocardium based on the metabolic signature of enhanced glucose metabolism in hypoperfused myocardium is the most prominent example used in cardiovascular investigation [36]. Some currently available radionuclide approaches to quantify key aspects of myocardial metabolism are summarized in Table 11.1 and will be described with examples of their application in cardiovascular investigation.

Table 11.1 Radiopharmaceuticals and ^{13}C-labeled compounds for cardiac metabolism

Metabolic process	Radiopharmaceutical[a]	^{13}C-labeled compound
Oxygen consumption	$^{15}O_2$, [1-^{11}C]acetate	[1-^{13}C]acetate, [2-^{13}C]pyruvate, [1-^{13}C]pyruvate
Long-chain fatty acid metabolism		
Uptake, oxidation, and storage	[1-^{11}C]palmitate, ^{18}F-F7, ^{123}I-IPPA[2]	
Uptake and oxidation	^{18}F-FTHA, ^{18}F-FTP,^{18}F-FTO, ^{18}F-FCPHA	
Uptake and storage	^{123}I-BMIPP[b]	
Short-chain fatty acid metabolism		
Acetylcarnitine metabolism	–	[1-^{13}C]acetate
Butyrate oxidation	–	[1-^{13}C]butyrate
Carbohydrate metabolism		
Uptake	^{18}FDG	
Uptake, glycolysis, oxidation	[1-^{11}C]glucose	
Lactate metabolism	[3-^{11}C]Lactate	
pH determination		
CO_2 – bicarbonate ratio		[1-^{13}C]pyruvate

[a]Abbreviations defined in text
[b]SPECT radiopharmaceutical

11.3.1 Single Photon Emission Computed Tomography

The advantages of SPECT for cardiac metabolic imaging include a wide distribution of the technology, the potential for multiphoton energy imaging permitting simultaneous assessment of multiple processes, and the long physical half-life of SPECT radiotracers which facilitates delivery of a radiotracer from a central radiopharmacy to multiple geographical locations. To determine the human relevance of the metabolic phenotypes of rodent models of various forms of cardiovascular disease, numerous small animal imaging SPECT and SPECT/CT systems have been developed. The major current disadvantage of SPECT is the inability to quantify cellular metabolic processes primarily because of the relatively poor temporal resolution of the technology. However, new designs in SPECT technology may permit dynamic data acquisitions allowing quantitative or semiquantitative measurements of substrate metabolism.

Currently, there are few available SPECT approaches for measuring myocardial metabolism. One of the earliest and most promising SPECT radiotracers of fatty acid metabolism was 15-(*p*-iodophenyl)-pentadecanoic acid (^{123}I-IPPA) [37–39]. This radiotracer demonstrated myocardial kinetics similar to ^{11}C-palmitate. However, the poor temporal resolution of SPECT systems could not take advantage of the rapid turnover of IPPA. However, the recent introduction of higher temporal resolution SPECT cameras may result in the reemergence of this radiotracer. Currently, the most widely used SPECT radiotracer is the alkyl branched-chain FA analogue, ^{123}I-beta-methyl-P-iodophenylpentadecanoic acid (^{123}I-BMIPP) (Fig. 11.1 and Table 11.1) [39–42]. Alkyl branching inhibits β-oxidation, shuttling the radiolabel to the TG pool, thereby increasing radiotracer retention and improving image quality. No specific SPECT radiotracers are currently available to measure myocardial glucose metabolism. However, when combined with the appropriate detection scheme and collimator design, myocardial glucose metabolism can be assessed with SPECT and ^{18}F-fluorodexoyglucose (^{18}FDG) [43].

11.3.2 Positron Emission Tomography

The major advantage of PET is a detection scheme that permits quantification of radioactivity within the field of view by utilizing radiotracers labeled with positron-emitting radionuclides. Several of these radionuclides are biologically ubiquitous elements such as oxygen (^{15}O), carbon (^{11}C), and nitrogen (^{13}N). Fluorine (^{18}F) can be substituted for hydroxyl groups which allow for its incorporation into a wide variety of substrates or substrate analogues that participate in diverse biochemical pathways. Moreover, because these radiotracers are administered at tracer doses, they do not alter the metabolic processes of interest (Tables 11.1 and 11.2). The general principle to quantify a myocardial metabolic process based on the tracer method is to measure both the delivery of material from blood, or input, and the tissue response. The latter represents the metabolic process of interest (Fig. 11.2). With PET, the radiolabeled metabolite-corrected input function is derived and used in conjunction with a mathematical model, or

Table 11.2 Summary of the effects of heart disease on myocardial substrate metabolism. Little is known about the effects of various disorders on ketone metabolism

	Fatty acids	Glucose	Pyruvate or lactate	Ketones
LV hypertrophy	↓	↑	↑	–
Ischemia	↓↓	↑	↓	↓
Insulin resistance and diabetes	↑	↓	–	–

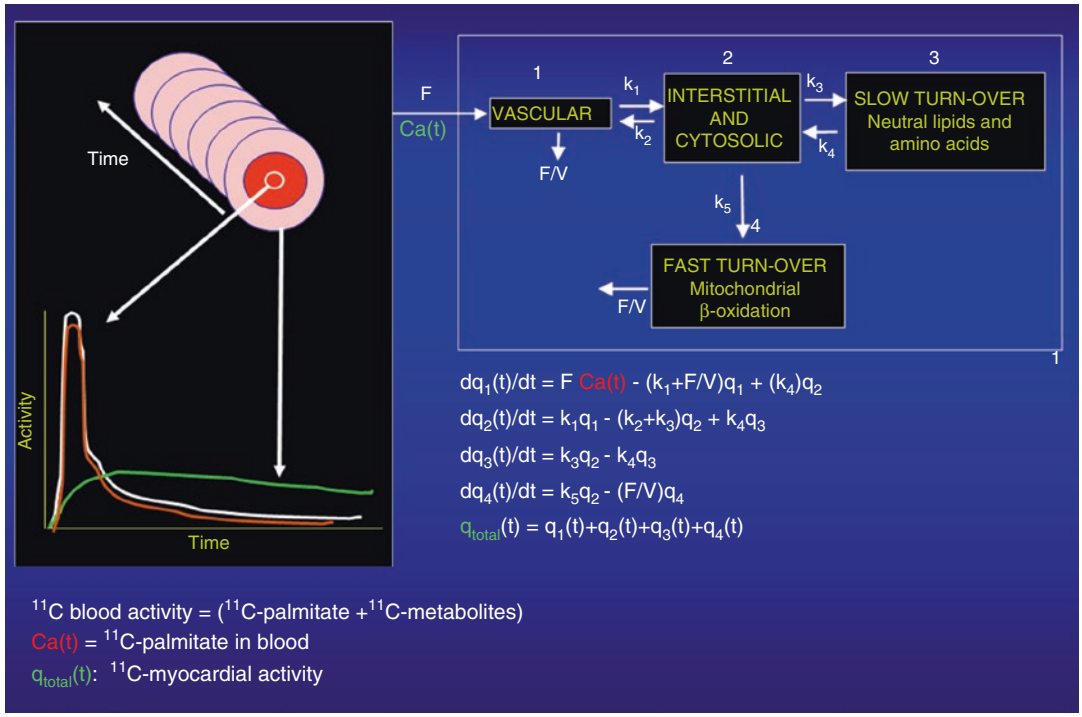

Fig. 11.2 Processes to quantify metabolic flux by PET. Shown here are the steps used to quantify flux through various pathways with PET using measurements of myocardial fatty acid with [1-^{11}C]palmitate as an example [59]. The left side of this figure again shows the conversion of idealized serial PET images from which both arterial and regional myocardial time-activity curves can be generated. The arterial time-activity curve is corrected for ^{11}C-labeled blood metabolites (in this case $^{11}CO_2$) to generate the arterial input function which reflects the delivery of [1-^{11}C]palmitate to the heart. The myocardial time-activity curve reflects the sum total of activity from all radiolabeled species in the myocardium. Movement of [1-^{11}C]palmitate into the myocardium is corrected for myocardial blood flow (F). The kinetic model for [1-^{11}C]palmitate has been divided into four key compartments of fatty acid metabolism with movement between the compartments determined by various rate constants (ks). The kinetic model fits the myocardial time-activity curve with the arterial input function to estimate the various rate constants. The rate constants are then included in the various differential equations to solve for different components of fatty acid metabolism

some variation, to quantify the metabolic processes by optimizing the model against PET-measured tissue response data (Fig. 11.2). Because of the poor spatial resolution of PET, both the input and tissue need to be corrected for geometric considerations such as partial volume and spillover effects. The measured tissue response in PET imaging reflects the sum total of radioactivity from all radiolabeled species in the tissue of interest. As such, the contribution of individual species and metabolic rates must be determined from the model parameters. PET cannot reliably characterize metabolism of substrates emanating from intracellular storage sites such as TG and glycogen pools. Other disadvantages of PET are its complexity in radiotracer design, image quantification schemes, and expense.

11.3.3 Myocardial Oxygen Consumption

Because oxygen is the final electron acceptor in all pathways of myocardial oxidative metabolism, PET with ^{15}O-oxygen has also been used

to measure myocardial oxygen consumption (MVO_2). The approach provides a measure of myocardial oxygen extraction which when combined with measurements of myocardial blood flow and arterial oxygen content directly measures MVO_2. Due to its short physical half-life, ^{15}O-oxygen is readily applicable in studies requiring repetitive assessments, such as those with an acute pharmacologic intervention. Its major disadvantages are the requirement for an on-site cyclotron, the need for a multiple tracer study to account for myocardial blood flow and blood volume, and the fairly complex compartmental modeling to obtain the measurements [44–46].

Acetate is a two-carbon fatty acid whose primary metabolic fate is rapid conversion to acetyl-CoA and metabolism through the TCA cycle. Because the TCA cycle and oxidative phosphorylation are tightly coupled, myocardial turnover of ^{11}C-acetate reflects overall oxidative metabolism or MVO_2. Either exponential curve fitting or compartmental modeling can be used to calculate MVO_2. Modeling is typically preferable when cardiac output is low because marked dispersion of the input function and spillover of activity from the lungs to the myocardium is present, which decreases the accuracy of the curve-fitting method [11, 47–50]. However, it is more complex than exponential curve fitting and requires correction of blood radioactivity for $^{11}CO_2$.

11.3.4 Carbohydrate Metabolism

^{18}F-Fluorodeoxyglucose, an analogue of glucose, is transported into the cytosol where it undergoes hexokinase-mediated phosphorylation. In general, ^{18}FDG-6-phosphate is trapped in the cytosol, and the myocardial uptake of ^{18}FDG is thought to reflect overall anaerobic and aerobic myocardial glycolytic flux [51–54]. Myocardial glucose uptake can be assessed in either relative or absolute terms (i.e., in nanomoles $\cdot$ g^{-1} $\cdot$ min^{-1}). For quantification, a mathematical correction called the "lumped constant" that accounts for the differences in glucose transport and hexokinase-mediated phosphorylation between FDG and glucose must be used to calculate rates of glucose uptake. This value may vary depending upon the prevailing plasma substrate and hormonal conditions, decreasing the accuracy of the measurement of myocardial glucose uptake [53, 55–57]. The limited kinetics of FDG in tissue precludes determination of the metabolic fate (i.e., glycogen formation versus glycolysis) of the extracted tracer and glucose.

Quantification of myocardial glucose metabolism has been performed with PET using glucose radiolabeled in the one-carbon position with ^{11}C, [1-^{11}C]glucose. Advantages of this approach include the lack of need for a lumped constant correction because [1-^{11}C]glucose is chemically identical to unlabeled glucose and thus has the same metabolic fate as glucose, more accurate measurements of myocardial glucose uptake compared with FDG, and the ability to estimate the metabolic fate of extracted glucose. Disadvantages of this method include a fairly complex synthesis of the tracer, the short physical half-life of ^{11}C (requiring an on-site cyclotron), compartmental modeling that is more demanding with ^{11}C-glucose than it is with FDG, and the need to correct the arterial input function for the production of $^{11}CO_2$ and ^{11}C-lactate.

Lactate metabolism in the heart can be measured with L-[3-^{11}C]lactate. A multi-compartmental model is used to estimate the extraction of lactate which correlates well with lactate oxidation measured by arterial and coronary sinus sampling over a wide range of conditions (Fig. 11.3) [58].

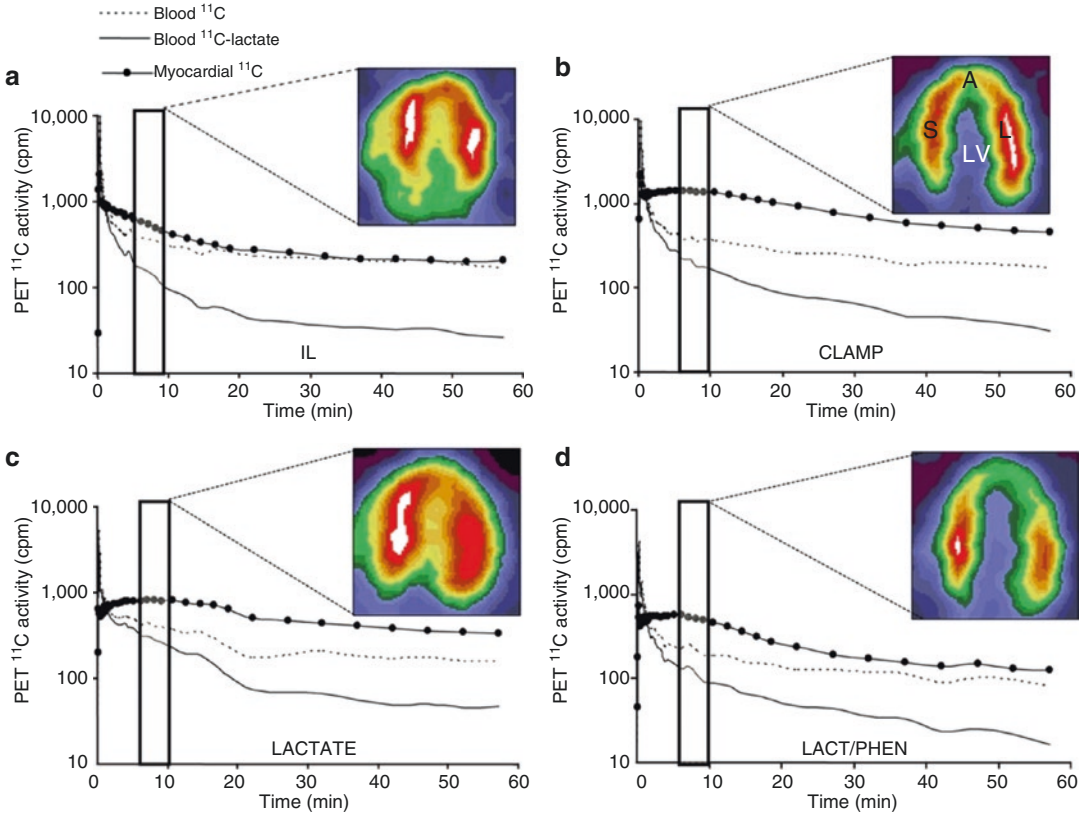

Fig. 11.3 PET measurement lactate metabolism. Representative PET time-activity curves of L-3-^{11}C-lactate obtained from intralipid (IL), insulin clamp (CLAMP), lactate infusion (LACTATE), or lactate and phenylephrine (LAC/PHEN) studies and corresponding myocardial images obtained 5–10 min after tracer injection and depicting primarily early tracer uptake. Images are displayed on horizontal long axis. Blood ^{11}C = ^{11}C time-activity curves obtained from region of interest (ROI) placed on the left atrium; blood ^{11}C-lactate = blood ^{11}C time-activity curves after removing $^{11}CO_2$, ^{11}C-neutral, and ^{11}C-basic metabolites; myocardial ^{11}C = ^{11}C time-activity curves obtained from ROI placed on the lateral wall. *A* apical wall, *S* septal wall, *L* lateral wall, *LV* left ventricle. Reproduced with permission Herrero P, et al. J Nucl Med. Dec 2007;48:2046-2055

11.3.5 Fatty Acid Metabolism

Palmitate is a saturated 16-carbon physiological long-chain fatty acid. A major advantage of [1-^{11}C]palmitate is that its myocardial kinetics including flux through β-oxidation and the TCA cycle are representative of oxidation of long-chain fatty acids. Currently, mathematical modeling techniques of the myocardial kinetics are used to measure various aspects of myocardial fatty acid metabolism uptake, oxidation, and storage [59–61]. The use of [1-^{11}C]palmitate does suffer from several disadvantages including suboptimal image quality, complex analysis, and the need for an on-site cyclotron and radiopharmaceutical production capability.

To increase the dissemination potential for measuring fatty acid metabolism, numerous

^{18}F- radiotracers have been developed. Most of the PET tracers in this category have been designed to reflect myocardial β-oxidation. The largest number of radiotracers has been developed as ^{18}F-radiolabeled thia fatty acids (Table 11.1). 14-(R,S)-^{18}F-fluoro-6-thiaheptadecanoic acid (^{18}FTHA) was one of the first radiotracers developed using this approach. Although in preclinical models myocardial uptake and retention tracked accordingly with changes in substrate delivery, blood flow, and workload, the uptake and retention of ^{18}FTHA were insensitive to the inhibition of β-oxidation by hypoxia [62–64]. To circumvent this problem, 16-^{18}F-fluoro-4-thia-palmitate (^{18}FTP) was developed and demonstrated a metabolic trapping function that is proportional to fatty acid oxidation under normal oxygenation and hypoxic conditions [64, 65]. Because fractional oxidation may be greater for oleate than for palmitate, a 4-thia-substituted oleate analogue 18-^{18}F-fluoro-4-thia-oleate (^{18}FTO) was recently developed [66]. In rat heart, FTO demonstrated a greater specificity for mitochondrial fatty acid oxidation and superior imaging characteristics than ^{18}FTP. Further studies are needed to confirm its utility in measuring myocardial FA metabolism in humans. The F-18-labeled fatty acid radiotracer, *trans*-9(*RS*)-^{18}F-fluoro-3,4(*RS*,*RS*) methylenehexadecanoic acid (^{18}FCPHA), a beta-methyl fatty acid analogue, has also been developed [67]. This radiotracer is also trapped after undergoing several steps of β-oxidation with uptake in rat heart approaching 1.5% injected dose per gram of tissue at 5 min postinjection. However, the impact of alterations in plasma substrates, work load, and blood flow on myocardial kinetics is unknown even though the radiotracer has undergone preliminary evaluation in humans [68]. There are some limitations with this class of radiotracers. Similar to ^{18}FDG, quantification of myocardial fatty acid metabolism requires the use of a lumped constant to correct for kinetic differences between the radiotracer and unlabeled palmitate. Furthermore, the extent to which myocardial fatty acid uptake can be separated from oxidation based on the myocardial kinetics of these radiotracers is unknown.

Other measurements of myocardial fatty acid metabolism are also accessible. Typically, PET measurements of myocardial FA metabolism only reflect the contribution of extracted FA bound to albumin or free fatty acids. However, myocardial fatty acid metabolism is dependent on the plasma delivery of fatty acid not just as free fatty acids but also in the form bound to TG, either as chylomicrons or very low-density lipoproteins. Fatty acids bound to TGs are made available to the myocardium via their release by lipoprotein lipase located on capillary endothelium. A noninvasive protocol for the assessment of TG-bound fatty acids has proven elusive. One proposed method to circumvent this problem is to administer the radiotracer orally to permit its incorporation into chylomicrons which can then be delivered to the heart. Using ^{18}FTHA, the approach has shown some promise in both rats and humans [69, 70]. Consistent with the mode of administration, most of the ^{18}F activities were recovered in the chylomicron fraction and with myocardial uptake occurring by 1 h and peaking 3 h post-administration. However, there remain technical challenges in quantifying the response from multiple sources of radiolabeled metabolites in the blood (radiolabeled TGs, chylomicrons, and nonesterified fatty acids), all of which contribute to the signal in PET imaging [71].

The contribution of intracellular or endogenous TG-derived fatty acids to overall energy metabolism appears to be altered in various animal models of cardiac disease such as heart failure and diabetes. However, relatively little is known about regulation of myocardial TG metabolism in humans [72, 73]. The lack of information is primarily due to the lack of adequate methods for its measurement [74, 75]. To help circumvent this problem, two strategies have been investigated. The first involves pre-labeling the myocardial TG pool with [1-^{11}C]palmitate, and once equilibrium is reached, measure the washout of activity under various substrate and hormonal conditions [76]. The approach was evaluated in dog heart where the rate of ^{11}C washout from the myocardium was correlated with arterial and coronary sinus measurements of the ^{11}C-metabolic species under varying metabolic conditions such as fasting and

hyperinsulinemic-euglycemic clamp with and without intralipid. However, the method suffers from the limitations of providing only an index of myocardial TG turnover and requiring the administration of a relatively high dose level of ^{11}C-plamitate which may preclude human use. A second approach to measure the turnover of the myocardial endogenous TG pool integrates the quantification of myocardial lipids by ^{1}H-MRS with PET-derived measurement (using [1-^{11}C] palmitate) of the oxidation rates for extracted fatty acids that either enter β-oxidation directly or after traversing the TG pool [77]. Using the method in obese humans demonstrated that the contribution to myocardial β-oxidation from fatty acids derived from intracellular TGs was at least equal to that of fatty acids extracted from plasma. The method is intriguing but does require validation with independent measurements of TG turnover. This is particularly important given the recent observations of the preferential oxidation of FAs derived from endogenous TGs compared with extracted fatty acids [9].

11.4 Hyperpolarized ^{13}C

The need for imaging specific metabolic pathways is clear from the complex interactions between disease and intermediary metabolism. Hyperpolarized ^{13}C technology takes advantage of the chemical specificity of ^{13}C NMR to probe multiple specific pathways plus the improved sensitivity afforded by various hyperpolarization methods. Dissolution dynamic nuclear polarization (DNP) is the most commonly used method to hyperpolarize ^{13}C, and its principles are summarized elsewhere [78–83]. The potential value of HP methods is illustrated in Fig. 11.4 where the kinetics of metabolism of HP[1-^{13}C]pyruvate to HP$^{13}CO_2$, HP[^{13}C]bicarbonate, [1-^{13}C]lactate and [1-^{13}C]alanine were monitored in a single exam of an isolated heart, enabling detection of flux through multiple pathways important in cardiac physiology.

Integration of hyperpolarized nuclei into a human imaging work flow will require the solution of three engineering problems. One problem is that instruments to generate hyperpolarized materials

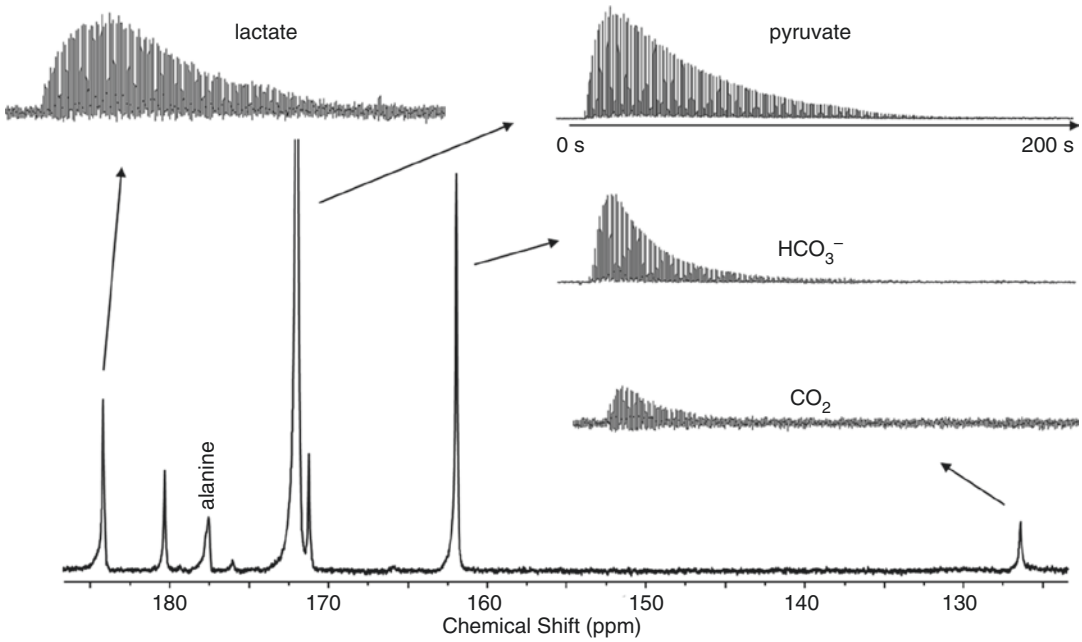

Fig. 11.4 ^{13}C NMR spectroscopy of an isolated rat heart. An isolated Langendorff-perfused rat heart was injected with hyperpolarized [1-^{13}C]pyruvate. Spectra were acquired every 2 s over an observation period of 200 seconds. Each inset is the ^{13}C NMR signal from a specific metabolite: lactate, pyruvate, bicarbonate, or CO_2. These spectra illustrate the rapid metabolism of [1-^{13}C]pyruvate to [^{13}C]CO_2 and other products. The total duration of data acquisition was 200 seconds. Data were redrawn from Merritt et al. Proc Natl Acad Sci USA. 2007; 104: 19,773-7

are prototypes with respect to clinical needs. A clinical instrument to rapidly and conveniently supply sterile, highly polarized (>80%) materials in sufficient mass for human exams is not available. A second challenge is that regardless of the details of the DNP process, once generated, the metabolite must be rapidly injected to minimize T_1 losses of polarization. Since the polarization state only exists in a magnetic field, it is essential to transfer the material from the site of generation to the subject through a slowly varying magnetic field. Passage through a region with zero field or a region with strong magnetic field gradients may eliminate polarization. Finally, optimal methods for data acquisition are necessary because once the hyperpolarized materials are no longer frozen at low temperatures, nuclear polarization will irreversibly decay to its thermal equilibrium value. One of the best molecules for HP exams is [1-^{13}C]pyruvate with a carbonyl T_1 of ~40 s, so there is generally a critical limit of 1–2 min for completion of the entire injection and image acquisition. Furthermore, the details of the imaging sequence are critical because each radiofrequency pulse depletes the available ^{13}C magnetization. The duration of available signal is therefore a combination of the nucleus (generally ^{15}N has a longer T_1 than ^{13}C), the chemical nature of the ^{13}C (generally carbonyls and carboxyls have a longer T_1 than protonated carbons), and the pulse sequence.

In addition to technical challenges, interpretation of ^{13}C-HP signals is not straightforward. Aside from technical issues, the ^{13}C NMR signal from any metabolite is proportional to [metabolite] (concentration of metabolite) · (fractional enrichment in ^{13}C) · (polarization). Consequently, for example, an increase in HP[1-^{13}C]lactate signal could be due to an increase in the pool size of lactate, an increase in the ^{13}C enrichment of the lactate pool, or an increase in the ^{13}C polarization as a consequence of better perfusion or more rapid transport of HP[1-^{13}C]pyruvate. In addition, it will be important to consider the multiple interacting biochemical events that could influence signals from HP products.

11.4.1 Probes and Pathways

The ideal ^{13}C-labeled probe for DNP must have four properties: safety after intravenous injection, long T_1, simple handling and efficient polarization, and rapid metabolism or the capacity to rapidly provide useful information. Characteristically these molecules are low molecular weight and water soluble. Thus an important challenge is to consider the metabolic pathway of interest and to match the possible probes to the pathway, as summarized in Tables 11.1 and 11.2. Glycolysis, for example, is important in understanding cardiac metabolism during ischemia, and it would be valuable to be able to compare studies of HP glucose to ^{18}FDG exams by PET. Glucose fulfills the other criteria: it is safe and water soluble and polarizes efficiently. However the T_1 of ^{13}C in glucose is short, on the order of a few seconds, so human imaging HP with glucose will be challenging, although not impossible. On the other hand, [1-^{13}C]pyruvate, [1-^{13}C]lactate, or [1-^{13}C]acetate all indirectly probe different aspects of glucose metabolism and offer simplicity, relatively long T_1 value, and the potential to probe important pathways. Unlike PET, multiple hyperpolarized ^{13}C probes may be injected in a single experiment. Multi-probe polarization or co-polarization refers to the simultaneous polarization of more than one probe as a single solution injection [84, 85]. This approach takes advantage of the chemical shift information encoded in the ^{13}C spectrum.

11.4.2 Pyruvate

Pyruvate is the reference molecule for DNP of the heart because of its central role in cardiac metabolism, convenience, ready polarization, and relatively long T_1 in carbons 1 and 2. [1-^{13}C] pyruvate is avidly metabolized in the heart to [1-^{13}C]lactate, [1-^{13}C]alanine, and [^{13}C]bicarbonate (Figs. 11.4 and 11.5); each product can be separately imaged in vivo because of the inherent chemical shift dispersion of ^{13}C [86–89]. Although interpreting each signal is a challenge because of the interacting effects of pool sizes and level of polarization, the capacity to image lactate, alanine, and bicarbonate provides direct information about key metabolic events in the heart. For example, the appearance of HP[1-^{13}C]lactate reflects activity of lactate dehydrogenase and the redox state of the cytosol. The appearance of HP[1-^{13}C]alanine reflects activity of another cytosolic enzyme,

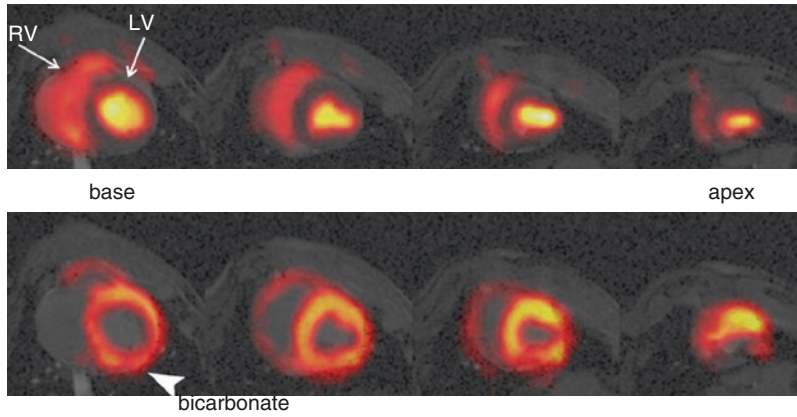

Fig. 11.5 Short axis hyperpolarized [1-^{13}C]pyruvate and [^{13}C]bicarbonate images of the pig heart. ^{13}C images were overlain on the corresponding anatomical images, arranged from the mid-left ventricle to the apex, left to right. In the upper panel, HP[1-^{13}C]pyruvate is seen filling the cavities of the right and left ventricles. In the lower panel, HP[^{13}C]bicarbonate was imaged throughout the left ventricular myocardium plus small regions of the right ventricular free wall. Redrawn from Dominguez-Viqueira et al. Magn Reson Med. 2016; 75: 859-65

alanine aminotransferase. Since activity of this enzyme is high and independent of redox potential, perhaps the HP[1-^{13}C]alanine signal reflects perfusion and transport of pyruvate. The decarboxylation of [1-^{13}C]pyruvate via PDH generates $^{13}CO_2$. Dissolved HP $^{13}CO_2$ may be directly detected in isolated rat [90] and mouse [18] hearts. In vivo, HP $^{13}CO_2$ exchanges rapidly with [^{13}C]bicarbonate via carbonic anhydrase and enables detection of flux through PDH. Since an HP exam can detect both dissolved HP $^{13}CO_2$ and [^{13}C]bicarbonate in the heart, pH can be calculated from the Henderson-Hasselbalch relationship [91]. The capacity to detect four specific enzyme-catalyzed reactions – pyruvate dehydrogenase, alanine aminotransferase, lactate dehydrogenase, and carbonic anhydrase – in a single exam illustrates the potential of HP technology.

One high-impact cardiac application of HP will likely be the detection of PDH flux; the biomarker in HP exams is the appearance of HP[^{13}C] bicarbonate from HP[1-^{13}C]pyruvate [90]. Noninvasive detection of flux through PDH would be of value in understanding heart disease because pharmacologic and metabolic interventions that target flux through PDH have been examined with the goal of protecting ischemic myocardium or improving function in the failing heart. Since ischemic heart disease is by definition a regional abnormality of perfusion due to coronary artery disease, the capacity for multislice imaging is critical for clinical translation and was demonstrated recently in a large animal model [88, 92] and illustrated in Fig. 11.5. Reduced [^{13}C]bicarbonate signal in hearts after coronary occlusion and reflow was previously attributed to an effect of transient ischemia on flux into the TCA cycle [86, 87].

[1-^{13}C]pyruvate also serves as an indirect probe of the TCA cycle because the HP products related to mitochondrial metabolism, $^{13}CO_2$ and [^{13}C]bicarbonate, are generated during flux through PDH. The product entering the TCA cycle, acetyl-CoA, is not ^{13}C labeled. Flux of pyruvate into the TCA cycle flux may be detected directly by placing the ^{13}C in position 2 of pyruvate (Fig. 11.6), which via PDH is converted to the product [1-^{13}C]acetyl-CoA. After condensation with oxaloacetate in the reaction catalyzed by citrate synthase, [5-^{13}C]citrate is produced. With further metabolism in the TCA cycle, α-ketoglutarate is produced and exchanges rapidly with glutamate; both metabolites are labeled in position 5 and glutamate can be detected [93, 94]. Since the biochemical pathways involved in [1-^{13}C]pyruvate and [2-^{13}C]pyruvate are identical, any difference in the rate of appearance of [^{13}C]bicarbonate from [1-^{13}C]pyruvate compared to the rate of appearance of [5-^{13}C]glutamate from [2-^{13}C] pyruvate presumably would be due to T_1 effects or metabolite pool sizes in the TCA cycle.

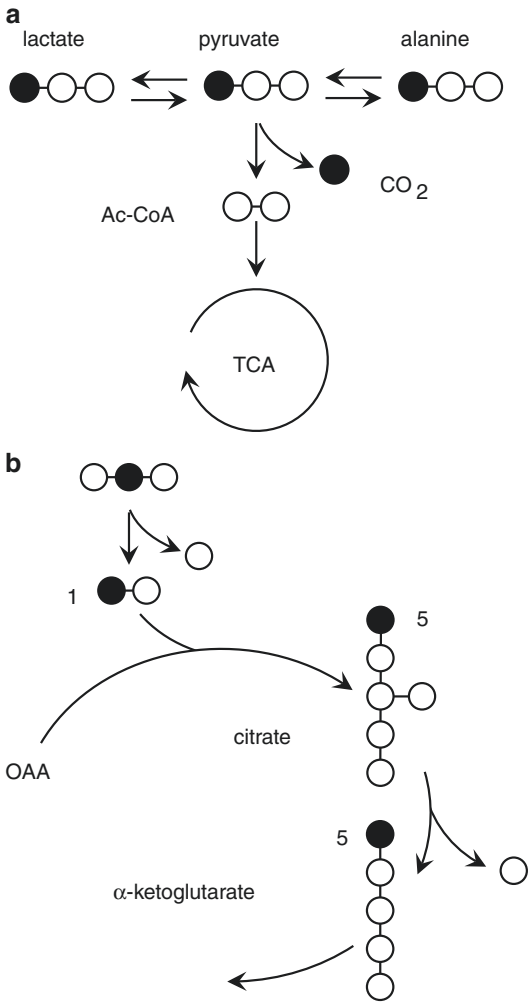

Fig. 11.6 Effect of ^{13}C labeling on detection of metabolism of pyruvate in the TCA cycle. Panel A illustrates conversion of [1-^{13}C]pyruvate to acetyl-CoA via pyruvate dehydrogenase with release of $^{13}CO_2$. PDH flux is detected directly from the appearance of $^{13}CO_2$ which is proportional to oxidation of pyruvate in the TCA cycle. Metabolism of [2-^{13}C]pyruvate in the heart, illustrated in Panel B, does not immediately yield $^{13}CO_2$, but ^{13}C will be transferred to position 5 of citrate and glutamate. Appearance of [5-^{13}C]glutamate directly demonstrates flux through citrate synthase

11.4.3 Lactate

As noted above, the ability to monitor flux through PDH may provide important information related to mitochondrial function. HP [1-^{13}C]pyruvate is safe in human subjects, but the endogenous plasma concentration is low. Therefore a bolus markedly alters plasma redox ratios, and arrhythmias have been reported at very high concentrations during intracoronary infusions. An alternative may be [1-^{13}C]lactate since lactate is also readily oxidized in the heart and the plasma concentration is roughly 10× pyruvate. Consequently, a bolus of an equivalent mass of lactate in principle has much less effect on redox potential. It is feasible to hyperpolarize [1-^{13}C]lactate using procedures similar to [1-^{13}C]pyruvate [95].

11.4.4 Acetate and Butyrate: Substrates That Bypass PDH

Pyruvate, in any of the labeling patterns described, is the reference molecule for DNP because of its central role in cell metabolism, ready polarization, and relatively long T_1 in carbons 1 and 2. However, fatty acids are the preferred substrate for energy production in the heart, and it would be ideal to probe TCA cycle metabolism directly. Acetate, the shortest chain fatty acid, is present only in low concentration in plasma but it is avidly oxidized by the heart. After conversion to acetyl-CoA by carnitine acetyltransferase, it also exchanges into acetylcarnitine. Thus, [1-^{13}C]acetate could in principle probe both the TCA cycle via metabolism to [5-^{13}C]glutamate and the kinetics of enrichment in acetylcarnitine [96, 97]. In healthy rats, HP[1-^{13}C]acetate was converted to both HP[1-^{13}C]acetylcarnitine and HP[5-^{13}C]citrate [97]. The kinetics of appearance of HP[1-^{13}C]acetylcarnitine have been studied in a pig model [98], but [5-^{13}C]glutamate could not be detected.

Fatty acid oxidation may be studied indirectly by examining the inhibition of pyruvate oxidation due to the presence of fatty acids. Hyperpolarized acetate bypasses PDH and may be considered a marker of fatty acid oxidation since it competes effectively against pyruvate and it interconverts with acetylcarnitine. However, because it bypasses β-oxidation, acetate fails to probe a key aspect of cardiac metabolism. [1-^{13}C]butyrate is a water-soluble four-carbon fatty acid that polarizes well. Normally it is present in very low concentrations in plasma and is thought to be derived from colonic

bacteria. Since [1-^{13}C]butyrate is metabolized through β-oxidation to [1-^{13}C]acetoacetyl-CoA and [1-^{13}C]acetyl-CoA (plus unlabeled acetyl-CoA), in principle [5-^{13}C]glutamate, [1-^{13}C]acetylcarnitine, and the redox pair, [1-^{13}C]acetoacetate and [1-^{13}C] beta-hydroxybutyrate, should all be detected. Indeed, this is the case in isolated perfused heart despite the hyperpolarized ^{13}C having passed through a minimum of nine enzyme-catalyzed reactions: [1-^{13}C]butyrate → [1-^{13}C]butyryl-CoA → [1-^{13}C]β-hydroxybutyryl-CoA → [1-^{13}C] acetoacetyl-CoA → [1-^{13}C]acetyl-CoA → [5-^{13}C] citrate → [5-^{13}C]isocitrate → [5-^{13}C]aconitate → [5-^{13}C]α-ketoglutarate → [5-^{13}C]glutamate [99].

11.4.5 Substrate Competition in Hyperpolarization Exams

The heart is exquisitely adapted to adjust fluxes in metabolic pathways almost instantaneously in response to changes in hemodynamic load as well as fluctuating concentrations of extracellular substrates. In general, an increase in extracellular concentration of a readily oxidized substrate is matched rapidly by an increase in oxidation of that substrate [105, 106]. This inherent flexibility of substrate selection is important in the design and interpretation of HP exams.

The normal concentration of pyruvate in plasma is ~0.1 mM, and pyruvate at this concentration contributes little to acetyl-CoA because of competing substrates [10]. Consequently, the capacity of the heart to rapidly switch to pyruvate, as after a bolus of HP[1-^{13}C]pyruvate, enables HP imaging of the heart. The rate of $^{13}CO_2$ production is proportional to the rate of acetyl-CoA production × the fractional contribution of [1-^{13}C]pyruvate to acetyl-CoA. Other factors being equal, the appearance of $^{13}CO_2$ or [^{13}C]bicarbonate in the heart is proportional to the fractional contribution of pyruvate to acetyl-CoA. Conversely, a high concentration of other circulating substrates, ketones, or fatty acids, for example, can inhibit oxidation of [1-^{13}C]pyruvate even in the high concentrations of pyruvate present after a bolus. In isolated hearts under conditions mimicking the fed state, 3 mM pyruvate was sufficient to produce ~80% of the acetyl-CoA [10]. At fatty acid and ketone concentrations present in fasting, pyruvate at 6 mM was oxidized at a significantly higher rate than at baseline, but oxidation of fats and ketones still provided the majority of acetyl-CoA. Consequently and not unexpectedly, the plasma concentration of HP [1-^{13}C]pyruvate (or other metabolizable substrate) will influence results. Further, the concentration of competing substrates will also influence pyruvate metabolism. Because the TCA cycle can oxidize acetyl-CoA from any source, there is no strict linkage between flux in the TCA cycle and flux in any one of the feeding pathways. Hence, the rate of appearance of HP $^{13}CO_2$ from HP[1-^{13}C]pyruvate may index flux through pyruvate dehydrogenase but not necessarily the TCA cycle.

11.5 Complementary Information

The purpose of this section is to consider how the unique and complementary attributes of PET and HP could be used to better understand myocardial metabolism. The first component will describe the potential for methodologic advancements, whereas the second component will provide a few examples where our understanding of metabolism could be enhanced.

PET provides the evolution over time of tissue radioactivity with very high sensitivity, measurable in three dimensions. Since the accessible information is total tissue radioactivity, detection of flux (in nanomoles · g^{-1} · min^{-1}) in a particular pathway relies on a tracer kinetic model that relates externally observed signal to an underlying metabolic network. Once the model is described mathematically and the relation between individual rate constants for each reaction and externally observed signal is established by validation experiments, typically performed in perfused tissues and large animal models, results from human patients can be derived. This approach, although well accepted, has several limitations. *First*, the arterial input function influences the kinetics of a tracer in heart muscle. The arterial input function is in turn sensitive to multiple factors including the cardiac output, the rate of tracer injection, and the mix of radiolabeled entities in the blood. *Second*,

kinetic models rely on knowledge of tissue metabolite pool sizes which, in the heart, are sensitive to normal physiological changes and disease. This limitation would presumably be most important for complex multi-compartment processes such as the oxidation of [1-^{11}C]acetate in the TCA cycle rather than the one-step phosphorylation of ^{18}FDG. In studies of MVO_2 over a wide range, an index of TCA cycle flux, there is a good correlation between the rate constant describing acetate oxidation and oxygen consumption, implying that the sum of metabolite concentrations involved in the TCA cycle remains more or less constant under normal physiological conditions. Nonetheless, the relevance of these measurements in healthy myocardium to patients with disease is uncertain. *Third*, it is difficult to build up experience in healthy volunteers or subjects with mild disease because of concerns related to exposure to ionizing radiation. Thus, much of the literature is based on patients with known significant heart disease.

In principle, MR imaging of hyperpolarized ^{13}C tracers overcomes some of these constraints. For example, after the injection of HP[1-^{13}C] pyruvate, the appearance of [1-^{13}C]lactate, [1-^{13}C] alanine, and [^{13}C]bicarbonate in the myocardium can only be interpreted as transit through lactate dehydrogenase, alanine aminotransferase, and pyruvate dehydrogenase, respectively, without the need for any mathematical models. Of course, conversion of HP-^{13}C signals to flux information will require kinetic models as well. Furthermore, the HP ^{13}C signal is depleted by the imaging sequence itself in a complex manner depending on the interpulse delay, flip angles, and whether individual metabolites are irradiated. Intracellular T_1 values in various tissue compartments are uncertain and perhaps even unknowable in intact tissues. If absolute flux information is desired, then all the factors that influence kinetic measurements by PET – the arterial input function and knowledge of tissue metabolite pool sizes – will be equally important for analysis of HP data.

11.5.1 Methodologic Advances

Based on the aforementioned discussion, it appears exploiting the complementary nature of PET and HP MR can provide potential advances. Perhaps PET can be used to help advance the quantitative capabilities of HP MR. For example, a properly calibrated arterial input function and tissue response on PET could be used as a gold standard to test the accuracy of new MR approaches that account for loss of polarization due to both the acquisition and the T_1 of the hyperpolarized molecule in order to derive similarly accurate measurements by HP MR, setting the stage for quantitative capability with this technology. Conversely, could knowledge of downstream metabolic partitioning of an extracted substrate measured with HP MR cross-validate a proposed mathematical model designed to interrogate certain metabolic pathways with PET? In addition, since PET measures myocardial metabolism without perturbing the system, it could be used to provide insight into the return of metabolic pathways of interest to baseline conditions following the administration of a ^{13}C HP molecule. Such information is fundamental to the successful advancement and application of serial HP MR studies. Finally, with the advent of PET/MR, it may be possible to link metabolic dose response by HP to the underlying baseline metabolic conditions measured by PET.

11.5.2 Applications and Potential Synergies

11.5.2.1 Myocardial Ischemia

The classic metabolic signature for myocardial ischemia is a decline in fatty acid uptake and oxidation and an increase in overall glucose metabolism via augmented anaerobic glycolysis and continued, albeit, diminished oxidative metabolism [107]. This metabolic switch permits continued energy production and cell survival in the setting of reduced tissue oxygen. However, unless NAD^+ can be regenerated by conversion of pyruvate to lactate and export of lactate, glycolysis will be inhibited by accumulation of NADH, and myocardial necrosis will ensue. When the ischemic insult is resolved, oxygen availability increases and oxidative metabolism resumes. Abnormalities in myocardial substrate metabolism present initially may persist well after the resolution of ischemia, a pattern termed "ischemic memory."

PET and SPECT

Demonstration of either accelerated myocardial glucose metabolism or reduced fatty acid metabolism using ^{18}FDG and ^{123}I-BMIPP, respectively, has been used to document ischemic memory. For example, over 20 years ago, it was shown that PET myocardial FDG uptake was increased in patients with unstable angina during pain-free episodes [108]. An example is shown in Fig. 11.7. Moreover, in patients with stable angina, increased FDG uptake was demonstrated following exercise-induced ischemia, in the absence of either perfusion deficits or ECG abnormalities [109]. Similar observations have been made with SPECT using ^{123}I-BMIPP. Results of numerous studies have

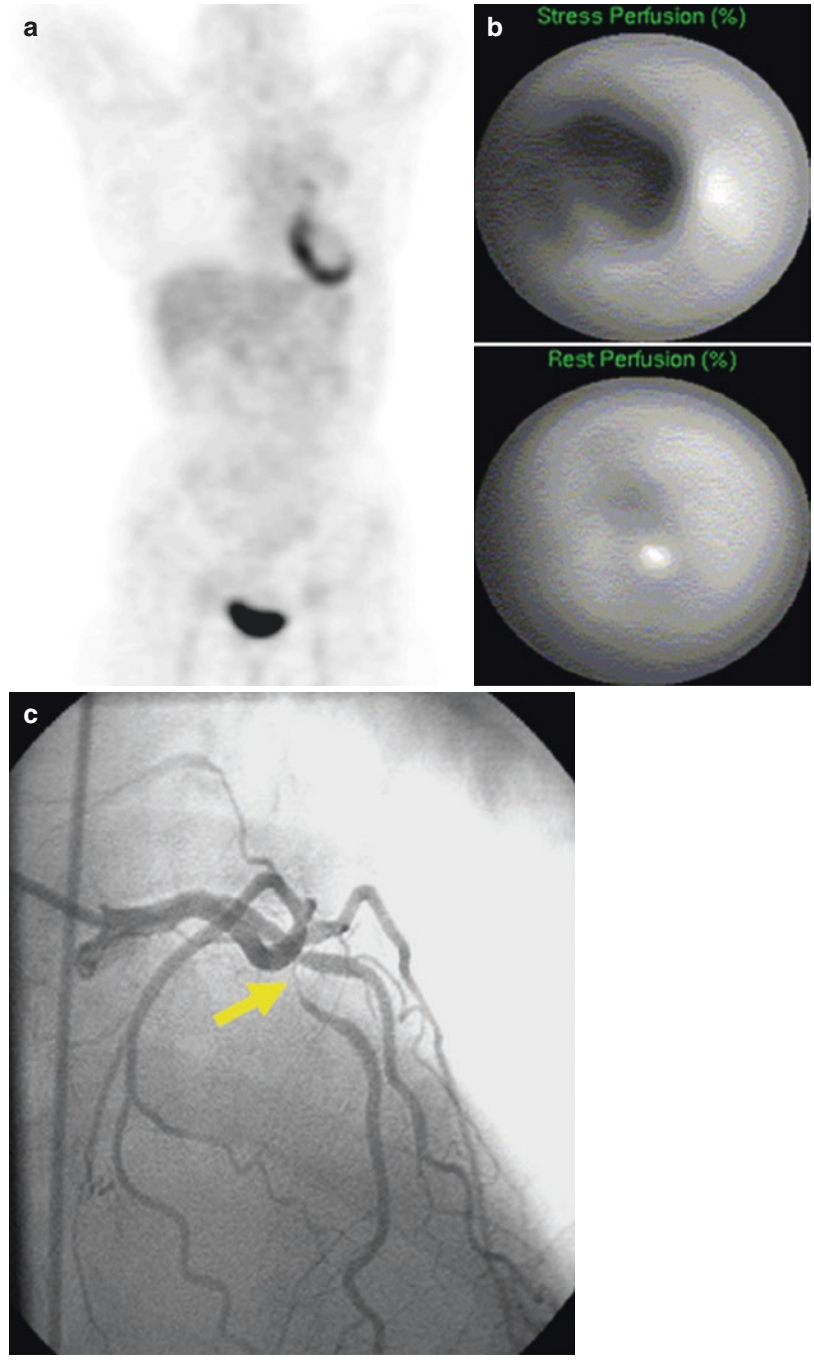

Fig. 11.7 Myocardial ischemia detected by FDG-PET. A patient with non-Hodgkin's lymphoma undergoing whole-body FDG-PET imaging for detection of recurrence. (**a**) Images acquired under fasting conditions demonstrate localized uptake in septal, anterior, and inferior walls of the myocardium, suggestive of either ischemia in these walls or infarction of the lateral wall. (**b**) Rest/stress SPECT myocardial perfusion imaging demonstrates inducible ischemia in the same distribution as the FDG uptake. (**c**) Coronary angiography demonstrates a high-grade stenosis in the left anterior descending artery (*yellow arrow*)

demonstrated in patients with acute chest pain that reductions in myocardial BMIPP uptake may persist 24–36 h following the resolution of symptoms [110, 111]. Moreover, this "metabolic fingerprint" may be superior to perfusion imaging for either identifying coronary artery disease as the cause of the chest pain or assigning prognosis [112]. It also appears that rest ^{123}I-BMIPP imaging may provide unique prognostic information in patients with end-stage renal dialysis receiving hemodialysis, a patient cohort with a high cardiovascular risk [113]. Metabolic imaging with either ^{18}FDG or ^{123}I-BMIPP has also been used for direct ischemia detection during stress testing. Abnormalities in vasodilator reserve with perfusion tracers will underestimate ischemia if oxygen and supply remain balanced. Results of initial studies where ^{18}FDG was injected during exercise demonstrated greater detection rate for moderately severe coronary artery stenoses compared with perfusion imaging [48, 114]. Despite the promising results with these radiotracers, numerous questions still remain such as the optimal imaging protocols and the impact of alterations in the plasma substrate environment on diagnostic accuracy, whether added diagnostic and prognostic information is provided over perfusion imaging and whether this information alters clinical management.

^{13}C Hyperpolarization

Clinicians can acquire detailed information about LV function and wall motion from MRI and echocardiography, but it may be difficult to readily identify the relations among symptoms, coronary anatomy, and the metabolic state of the tissue and to predict the likely outcome after revascularization. The promise of HP methods to probe myocardial ischemia arose early in its development [91, 92]. In isolated hearts where the timing of ischemia, reperfusion, and delivery of HP[1-^{13}C]pyruvate can be controlled, there is already evidence that spectra of the products [1-^{13}C]lactate, $^{13}CO_2$, and [^{13}C]bicarbonate can provide highly specific information about myocardial ischemia. Necrotic myocardium cannot produce lactate, CO_2, or bicarbonate from HP [1-^{13}C]pyruvate. Brief ischemia not sufficient to cause irreversible injury was associated with rapid recovery of high-energy phosphates, mechanical function, and oxygen consumption [115]. Yet even under these conditions where conventional physiological studies indicate that the myocardium is "normal," the HP ^{13}C NMR spectrum was dramatically abnormal. Flux through PDH was undetectable, and the concentration of lactate was dramatically increased, likely due to the strongly reducing environment in both the mitochondria, causing inhibition of PDH, and in the cytosol, causing accumulation of lactate. This profile, absent bicarbonate and abnormally high lactate, demonstrates that the cardiomyocytes were functional in the sense that pyruvate is being delivered to the cells and that lactate dehydrogenase is highly active. Thus, a low ratio of HP bicarbonate to HP lactate appears to indicate recent brief ischemia when all other conventional measures are normal.

The effects of brief (15 min) or prolonged (45 min) occlusion of the circumflex coronary artery followed by reperfusion were examined in a pig model in vivo [92]. Ejection fraction was not measurably altered in this study, indicating that the volume of ischemic myocardium was relatively small, and the concentration of creatine kinase MB was elevated after 45 min but not after 15 min of ischemia. Delayed enhancement after Gd was not detected after brief ischemia. Nevertheless (Fig. 11.8) a small but distinct volume of reduced HP [^{13}C]bicarbonate was observed in the circumflex territory 2 h after reperfusion. The HP[1-^{13}C]alanine image was not influenced by brief ischemia. This study demonstrated that while a map of perfusion and cytosolic function, HP[1-^{13}C]alanine, was normal after brief ischemia with 2 h of reperfusion, the HP[^{13}C]bicarbonate image was abnormal. This finding illustrates the potential sensitivity of HP methods for ischemia and is an example of ischemic memory: metabolism was abnormal even when perfusion and function were apparently preserved.

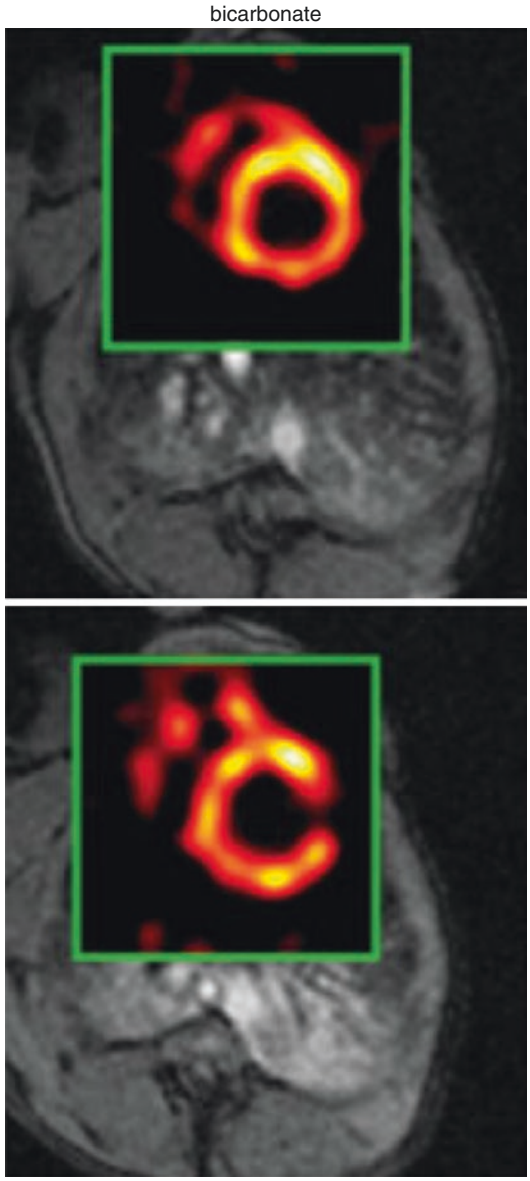

Fig. 11.8 Influence of brief ischemia in the circumflex territory on appearance of hyperpolarized [^{13}C] bicarbonate. The left circumflex artery of a pig was occluded for 15 min followed by 2 h. of reperfusion and intravenous injection of HP[1-^{13}C]pyruvate. The bicarbonate signal in the circumflex territory was significantly reduced. Images from Golman et al. Magn Reson Med. 2008; 59: 1005-13

Potential Synergies

The metabolic fate of a carbohydrate is very sensitive to normal physiological changes and pathological conditions; a good example is oxidation of glucose via glycolysis in the TCA cycle under normal aerobic conditions compared to export as lactate during ischemia. ^{18}FDG accumulates prior to the split between aerobic and anaerobic carbohydrate metabolisms and therefore cannot distinguish these pathways. Preserved uptake of ^{18}FDG and trapping as a phosphorylated product indicate ischemic myocardium, but it is not known if this biomarker is detecting preserved mitochondrial metabolism (glucose → pyruvate → CO_2) or preserved cytosolic functions (glucose → lactate). Having the capability to measure the proportional contributions of the cytosolic and mitochondrial partitioning of glucose metabolism (measured by ^{13}C-HP) normalized to overall glucose metabolism (measured with PET and ^{18}FDG) would permit delineation of the relative importance of these two pathways in maintaining cardiomyocyte health in humans with coronary artery disease, perhaps laying the foundation for novel clinical management paradigms.

11.5.2.2 Myocardial Hypertrophy and Cardiomyopathies

The metabolic phenotype of a reduction in the expression of β-oxidation enzymes, leading to a fall in myocardial fatty acid oxidation and an increase in glucose use, characterizes both LV and right ventricular (RV) hypertrophy [116–119]. This adaptive response is considered beneficial to cardiac function under acute conditions, but under exposure to sustained pressure overload, the metabolic switch becomes more permanent, impairing flexibility in myocardial substrate use and inducing mitochondrial dysfunction [120]. Indeed, interventions in animals that involve inhibition of mitochondrial fatty acid β-oxidation result in cardiac hypertrophy [116]. Further support for this linkage arises from observations in humans, where variants in genes regulating key aspects of myocardial fatty acid metabolism ranging from PPARα to various key β-oxidative enzymes are associated with LV hypertrophy [121, 122].

In addition to LV hypertrophy, alterations in myocardial substrate metabolism have been implicated in the pathogenesis of contractile

dysfunction and heart failure. Animal models of heart failure have shown that in the progression from cardiac hypertrophy to ventricular dysfunction, the expression of genes encoding for enzymes regulating β-oxidation is coordinately decreased, resulting in a shift in myocardial substrate metabolism to primarily glucose use, similar to that seen in the fetal heart [123, 124]. The reactivation of the metabolic fetal gene program may have numerous detrimental consequences on myocardial contractile function ranging from energy deprivation to the inability to process fatty acids leading to accumulation of nonoxidized toxic fatty acid derivatives, resulting in lipotoxicity. It should be noted this metabolic adaptation becomes more complex when there is concomitant insulin resistance [125].

SPECT and PET

In preclinical models of LV hypertrophy, PET with FDG has demonstrated that myocardial glucose uptake tracks directly with increasing hypertrophy and provides evidence that metabolic changes are one of the first myocardial responses to increased stress, and these metabolic adaptations may drive the hypertrophic response with respect to its functional and structural consequences [126–130]. Similar results have been found in man. PET with [1-^{11}C]palmitate in humans has shown the reduction in myocardial fatty acid oxidation is an independent predictor of LV mass in hypertension [131]. Measurements of myocardial glucose metabolism with PET and ^{18}FDG and myocardial structure and function by echocardiography were performed in a cross-sectional study of normal controls and hypertensive patients without or with LV hypertrophy [132]. Consistent with the aforementioned observations obtained in preclinical studies, the rate of myocardial glucose uptake PET was higher in patients without LV hypertrophy compared with controls suggesting the metabolic remodeling preceded structural remodeling in these patients. But surprisingly, the rate of myocardial glucose uptake was lower in hypertensive patients with LV hypertrophy when compared with the hypertensive patients without LV hypertrophy. Furthermore, it appeared the decline in the rate of glucose uptake paralleled the decline in diastolic function. These latter findings are at odds with preclinical observations and may be attributable to the greater preponderance of females and diabetics in the LV hypertrophy cohort.

Similar observations of increased myocardial ^{18}FDG uptake have been obtained in patients with RV hypertrophy due to pulmonary hypertension [133–135]. The increase in ^{18}FDG uptake correlates with the level of pulmonary hypertension, plasma NT-pro-brain natriuretic peptide levels, as well as circulating levels of bone marrow-derived proangiogenic progenitors (CD34+ and CD133+ cells) which are markers of generalized hypoxia-inducible factor 1-alpha activation, a known driver of the hypertrophic response [133]. Moreover, an increase RV glucose uptake appears to be a marker of poorer prognosis [135, 136]. It also appears that measuring RV ^{18}FDG uptake can be used to follow therapeutic responses as treatment of pulmonary hypertension (e.g., epoprostenol or sildenafil) results in a decline in pulmonary hypertension that is paralleled by a decrease in RV myocardial glucose uptake [135, 137]. Finally, alterations in RV myocardial metabolism also occur in RV dysfunction, secondary to left heart failure [138].

In summary, these studies raise the possibility of using metabolic imaging for both prognosis assignment and treatment monitoring for patients with pressure-overload conditions of either the left or right ventricle. However, they also highlight the complexity of metabolic imaging and the need to control the many determinants of myocardial metabolism in order to accurately attribute a unique metabolic signature to a specific disease process.

SPECT with BMIPP has demonstrated reduced myocardial uptake and increased radiotracer clearance in patients with dilated cardiomyopathy compared with controls [139]. Moreover, the magnitude of these metabolic abnormalities correlated with other measurements of severe heart failure such as left ventricular size and plasma β-natriuretic peptide levels. It appears these abnormalities in BMIPP kinetics reflect the combined effects of reduced fatty acid uptake and oxidation as evidenced by PET with [1-^{11}C]palmitate studies in a similar patient population. In this same study, myocardial glucose metabolism was higher in the cardiomyopathic patients compared with controls confirming the

metabolic shift [140]. Moreover, it appears sex impacts the metabolic phenotype in nonischemic cardiomyopathy with women exhibiting higher levels of myocardial fatty acid uptake (and blood flow) compared with males as measured by PET using [1-^{11}C]palmitate (Fig. 11.9) [141]. However, it should be noted that the presence of concomitant insulin resistance appears to be a major contributor to the variability in levels of myocardial glucose and fatty acid metabolism in these patients [142, 143].

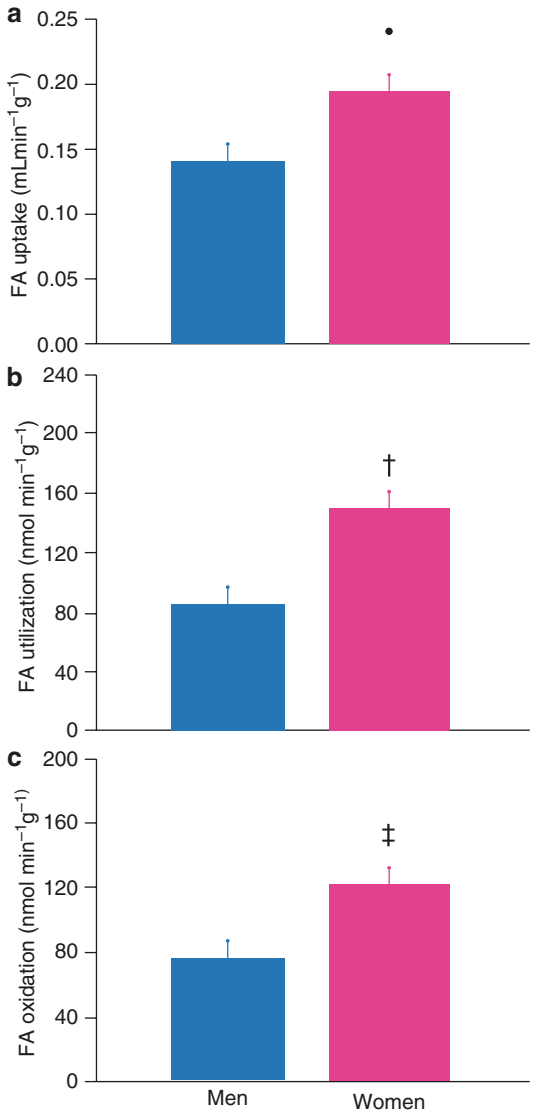

Fig. 11.9 PET measurements in nonischemic cardiomyopathy. Sex differences in myocardial fatty acid (FA) uptake and metabolism in heart failure. Myocardial FA uptake (**a**), utilization (**b**), and oxidation (**c**) averages in men (*blue bars*) and women (*pink bars*) with nonischemic heart failure. Reproduced with permission Kadkhodayan A, et al. J Nucl Cardiol. 2016;epub

Metabolic imaging can also be used to study the mechanisms responsible for the effectiveness of treatment in dilated cardiomyopathy. For example, the administration of the nonselective β-blocker, carvedilol, results in a 20% decline in myocardial fatty acid uptake [144]. Theoretically, decreasing myocardial fatty acid oxidation should increase the oxidation of glucose leading to a more favorable energetic state and improved LV function. Alterations in myocardial substrate use are now becoming attractive targets for novel treatments for heart failure with prime examples being the partial fatty acid oxidation antagonists and the insulin sensitizer glucagon-like peptide-1 [145, 146]. The administration of trimetazidine to patients with dilated cardiomyopathy resulted in a significant improvement in LV ejection fraction [147]. However, the improvement in LV function appeared to reflect the complex interplay between a mild decrease in myocardial FA oxidation, improved whole-body insulin resistance, and synergistic effects with β-blockade. More recently the effects of the GLP-1 agonist, albiglutide, on myocardial glucose and oxidative metabolism were assessed with PET and ^{18}FDG and [1-^{11}C]acetate, respectively, in patients with NYHA Class II–III heart failure. Although there was no detectable effect of albiglutide on cardiac function or myocardial glucose and oxygen use, there was a modest increase in peak oxygen consumption, which could have been mediated by noncardiac effects [148]. However, the study does highlight the potential of PET-derived metabolic biomarkers as endpoints for CV drug development.

^{13}C Hyperpolarization

Even at this relatively early stage in the development of technology for HP studies, preclinical models of heart failure have been examined. Hypertrophy, induced by thyroxine administration in rats, was associated with a reduction in PDH flux measured by metabolism of HP[1-^{13}C] pyruvate [149]. Pacing-induced dilated cardiomyopathy was examined over time in a pig model [94]. Early in the period of rapid pacing, HP[^{13}C] bicarbonate production from HP-[1-^{13}C]pyruvate was preserved (Fig. 11.10). The metabolism of

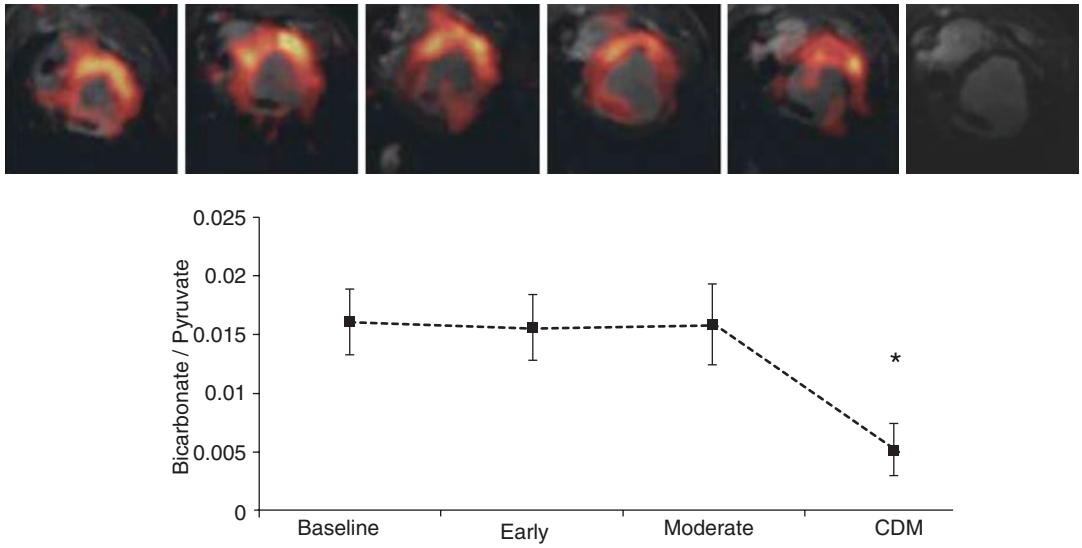

Fig. 11.10 Influence of pacing-induced dilated cardiomyopathy on appearance of hyperpolarized [^{13}C] bicarbonate. ^{13}C MR images were taken from the same pig at weekly intervals during the evolution of a dilated cardiomyopathy (DCM) induced by rapid pacing. *Upper panel*: The appearance of HP[1-^{13}C]bicarbonate was preserved in the left ventricular myocardium until late in the progression to heart failure. *Lower panel*: Bicarbonate signal normalized to pyruvate. "Early" and "moderate" refer to the duration of pacing, 1–2 weeks and 2–5 weeks, respectively. DCM refers to the appearance of overt heart failure. Data from Schroeder et al. Eur J Heart Fail. 2013; 15: 130-40

HP[2-^{13}C]pyruvate was used to examine production of [5-^{13}C]glutamate in the TCA cycle to directly probe citrate synthase. Surprisingly, the signal of HP[5-^{13}C]glutamate decreased early during hemodynamic stress, demonstrating a dissociation between bicarbonate production from [1-^{13}C]pyruvate and [5-^{13}C]glutamate production from [2-^{13}C]pyruvate. It is conceivable that mitochondrial water content or other structural changes may modify the T_1 of metabolites early in the citric acid cycle, or exchange of metabolite upstream from α-ketoglutarate may delay the transfer of HP [1-^{13}C]acetyl-CoA to glutamate. These data suggest that an integrated investigation using HP probes could provide new insights into the pathophysiology of heart failure.

Potential Synergies

PET with [1-^{11}C]acetate has been investigated extensively as a tool to measure myocardial oxygen consumption [52, 53, 64, 150–152]. A challenge is that regional measurements of acetate clearance are converted to oxygen consumption or, equivalently, TCA cycle flux by a predetermined relationship. However, it is not feasible to model all possible conditions that may influence that relationship. The use of HP [1-^{13}C]acetate to assess TCA cycle flux is attractive because the signal from HP[5-^{13}C]citrate can be resolved from the acetate signal in perfused heart models, and kinetic analyses have been reported. Interestingly, several reports described metabolism of hyperpolarized [1-^{13}C]acetate → [1-^{13}C] acetyl-CoA → [1-^{13}C]acetylcarnitine in a reaction catalyzed by carnitine acetyltransferase [102, 103, 153]. The buffering capacity of the carnitine-acetylcarnitine system has not been incorporated in PET kinetic models. As anticipated, both [1-^{13}C]acetylcarnitine and [1-^{13}C] butyrylcarnitine are detected in the presence of HP[1-^{13}C]butyrate [154].

The ability to distinguish metabolism of acetate via oxidative metabolism vs. entry into the acetylcarnitine pool may be important in myopathies. Carnitine is absolutely required for normal oxidation of fatty acids in the heart, and abnormalities of carnitine metabolism have been associated with heart failure [155] or abnormal

mitochondrial function in the heart [156, 157]. Reports of heart failure are presumably due to interference with fatty acid oxidation. Dietary carnitine supplementation has been suggested in heart failure [158]. Since the conversion of hyperpolarized [1-^{13}C]acetate to [1-^{13}C]acetylcarnitine is readily detected, HP methods may prove useful in understanding carnitine metabolism and indirectly fatty acid metabolism. As described previously, metabolism of hyperpolarized [1-^{13}C] butyrate into the TCA cycle also provides information about TCA cycle kinetics [104].

11.5.2.3 Obesity, Insulin Resistance, and Diabetes

Obesity is a major risk factor for heart failure [159]. Moreover, it appears an "obesity cardiomyopathy" is a distinct clinical entity characterized by LV remodeling, reduced cardiac efficiency, and diastolic dysfunction, which may progress to systolic dysfunction [160]. The mechanisms responsible for the relation between obesity and heart failure in humans are not well understood but may, in part, involve altered myocardial substrate metabolism. Preclinical models demonstrate obesity increases myocardial fatty acid metabolism, lipid accumulation, and MVO_2 leading to increased oxidative stress, cardiac dysfunction, and apoptosis [161, 162]. Interventions that reduce fatty acid accumulation and/or oxidative stress in cardiac myocytes prevent the development of myocardial dysfunction in these models [161].

Overdependence on fatty acid metabolism and a decrease in glucose use typifies the metabolic phenotype in diabetes mellitus [163, 164]. The increase in plasma fatty acid delivery due to peripheral insulin resistance leads to increased myocardial fatty acid uptake. This activates key transcriptional pathways such as the PPARα/PGC-1 signaling network resulting in a further increase in myocardial fatty acid uptake and oxidation with reciprocal reduction in glucose oxidation [165–167]. However, additional mechanisms are also likely at play. Insulin-mediated stimulation of glucose transport is impaired by intramyocardial lipid accumulation likely through activation of various isoforms of protein kinase C [168–170]. Excess fatty acid oxidation may also be associated with a decrease in the metabolic flexibility of the heart which as noted above is a characteristic of the normal myocardium [171, 172]. Through poorly understood mechanisms, increased fatty acid oxidation is associated with excess myocardial oxygen consumption [173–178]. This effect is generally modest, perhaps an increase in oxygen consumption of a few percent up to 30% for the same myocardial work. This change is much less than the normal variation in oxygen consumption by the heart during minimal exercise. However under perfusion-limiting conditions such as ischemic heart disease or with impaired subendocardial capillary flow during hypertrophy, this effect is conceivably significant. Moreover, these chronic metabolic adaptations can initiate a cascade of events that acting either individually or synergistically are detrimental to cardiac myocyte health such as an increase in oxidative stress, inflammation, and increased cell death, all of which can lead to diastolic dysfunction [163, 166].

PET

Imaging of obese young women with PET and [1-^{11}C]acetate and [1-^{11}C]palmitate has demonstrated that an increase in body mass index is associated with a shift in myocardial substrate metabolism toward greater fatty acid use that increased with worsening insulin resistance [173]. Of note, little change in myocardial glucose metabolism was observed. Paralleling the preferential use of FAs was an increase in MVO_2 and a decrease in energy transduction. The myocardial metabolic response to obesity appears to be sex dependent. For example, using similar PET techniques, it has been demonstrated that in contrast to obese women, obese men have a greater impairment in myocardial glucose metabolism [179, 180]. In addition, obesity had less effect on myocardial fatty acid metabolism in men. In contrast, MVO_2 was higher in the obese women compared with obese men. PET studies have now documented the salutary effects of weight loss on myocardial metabolism, structure, and function [181, 182].

Small animal PET imaging has helped clarify the mechanisms responsible for the metabolic alterations that occur in diabetes mellitus. For example, PET studies with [1-^{11}C]palmitate and FDG in relevant genetic models demonstrate that PPARα and PPARβ/σ drive different metabolic regulatory programs in the diabetic heart [183, 184]. In a more clinically relevant model of type 2 diabetes mellitus, the Zucker diabetic fat rat, myocardial glucose uptake correlates directly and closely with GLUT 4 gene expression, demonstrating the quantitative capability of the technique [185]. PET measurements in the same model demonstrated a decline in myocardial glucose uptake and an increase in fatty acid uptake and oxidation. The metabolic adaptations were associated with a decline in insulin-mediated phosphorylation of Akt which is indicative of reduced insulin action and an increase in abundance at the sarcolemma of the fatty acid transporter CD36, respectively [186]. Of note, these PET techniques have now been optimized for mouse heart [187].

The results of several imaging studies in humans have generally reproduced the observations from preclinical studies and as a result greatly expanded our understanding of the chronic metabolic adaptations in the diabetic heart. PET and [1-^{11}C]palmitate and [1-^{11}C]glucose in patients with type 1 diabetes mellitus demonstrate higher levels of fatty acid uptake and oxidation compared with nondiabetics primarily due to increased plasma FA levels. In contrast, glucose uptake is reduced in these patients primarily due to decreased glucose transport mechanisms [65]. Moreover, the metabolic fate of extracted glucose is impaired in diabetes with reduced rates of glycolysis and glucose oxidation which become more pronounced with increases in cardiac work induced by dobutamine [188]. However, the myocardium in type 1 diabetic patients is responsive to changes in plasma insulin and fatty acid levels but at a cost. Higher insulin levels are needed to achieve the same level of glucose uptake and glucose oxidation compared with nondiabetics, consistent with myocardial insulin resistance. Similarly, in response to higher fatty acid plasma levels, myocardial fatty acid uptake is increased at the cost of a greater esterification rate [189].

Results of metabolic imaging studies in patients with type 2 diabetes mellitus that were composed of various combinations of PET, ^{1}H-MRS, ^{31}P-MRS, MRI, and echocardiography have yielded remarkably consistent results that in general parallel preclinical observations and support the mechanistic framework for diabetes-induced chronic metabolic adaptations. These observations include a systemic environment typified by reduced whole-body insulin sensitivity and increased plasma fatty acid and TG levels that is paralleled by a PET-derived myocardial metabolic profile that includes increased fatty acid uptake and oxidation and reduced glucose uptake, the magnitude of which is dependent upon whether the measurements are performed in the fasted state or during insulin clamp [190–193]. In general, results of ^{1}H-MRS studies demonstrate an increase in myocardial lipid content and decline in energetics that are associated with LV diastolic and in some cases systolic dysfunction [194–196]. It appears changes in the myocardial metabolic-functional relationship parallel the progressive worsening in the systemic profile as one transitions from a lean condition to obesity without diabetes to concomitant obesity [191, 193]. It also appears the sexual dimorphism in myocardial metabolism that exists in lean subjects and obese nondiabetics is present in patients with concomitant obesity and type 2 diabetes mellitus. In these patients, women appear to have more pronounced augmentation in myocardial fatty acid metabolism and a greater propensity to form TG compared with diabetic men [191]. In contrast, diabetic men appear to have a greater impairment in myocardial glucose uptake and oxidation compared with diabetic women (Figs. 11.11 and 11.12) [180]. These results are intriguing given the greater susceptibility of females with type 2 diabetes mellitus to develop heart failure and exhibit a poorer prognosis when compared with male diabetics [197–199].

The effects of antidiabetic therapies in humans on myocardial metabolism have been evaluated by PET. For example, differential effects of the PPARγ agonists pioglitazone,

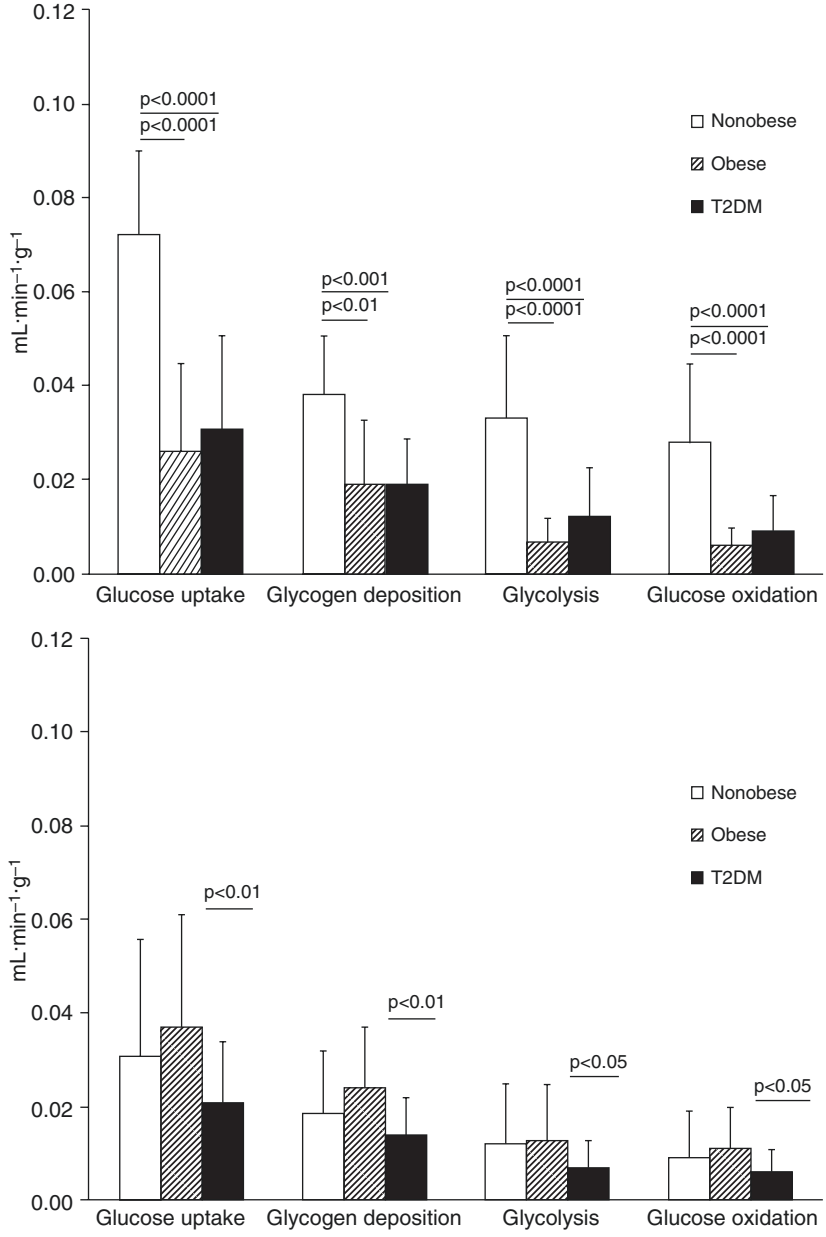

Fig. 11.11 Sexual dimorphism in myocardial metabolism in obesity and diabetes. Measurements of the fractional uptake of glucose, glycogen deposition, glycolysis, and oxidation measured by PET with [1-^{11}C]glucose in lean, obese, and diabetic men (*Top*) and women (*Bottom*). Data suggest that men exhibit a greater decline in glucose metabolism compared with women as one transitions from lean to obese to diabetes. Reproduced with permission Peterson LP et al., Am J Physiol Heart Circ Physiol 308: H1510–H15

rosiglitazone, and the biguanide and metformin on myocardial glucose and fatty acid metabolism have been assessed using PET with FDG or [1-^{11}C]glucose and [1-^{11}C]palmitate, respectively. Treatment with either rosiglitazone or pioglitazone results in an increase in insulin-stimulated myocardial glucose uptake. In contrast, insulin-stimulated myocardial glucose uptake is either unchanged or reduced with metformin therapy [200, 201]. In male diabetics,

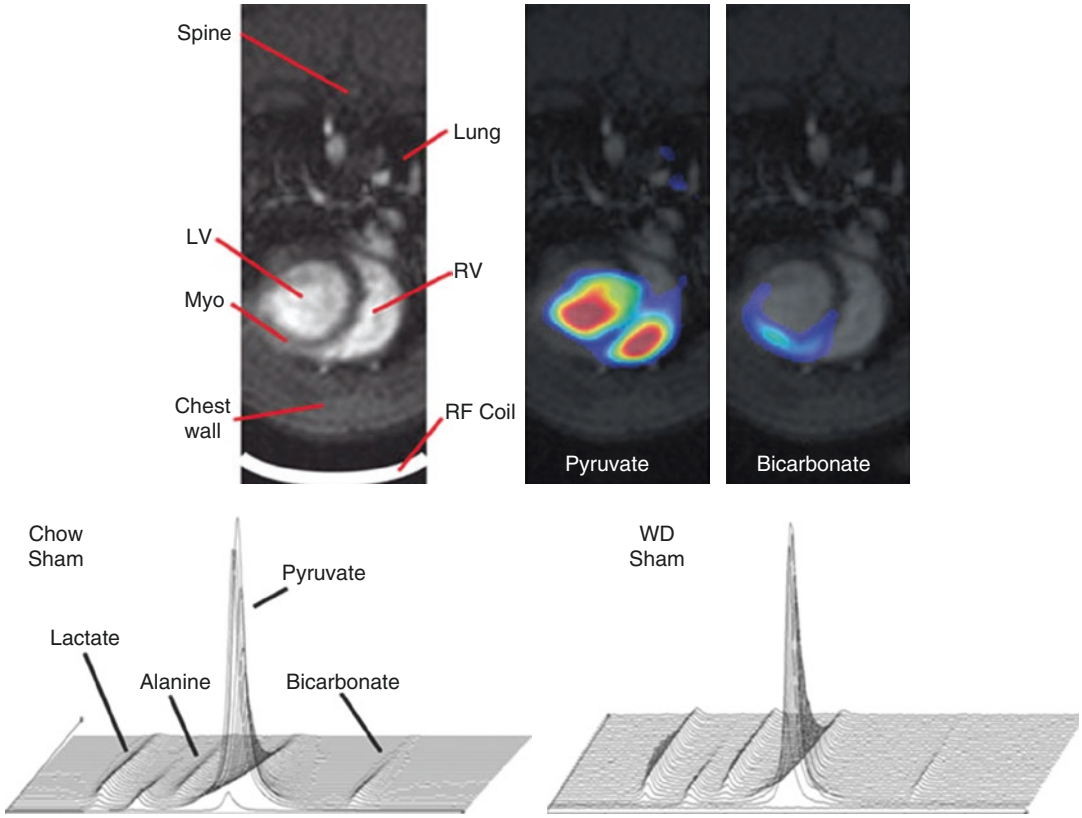

Fig. 11.12 Effects of a Western diet on appearance of hyperpolarized [^{13}C]bicarbonate in the rat heart. *Upper panel* shows, left to right, a conventional MRI, a ^{13}C MR image of pyruvate in the right and left ventricular cavities, and a ^{13}C MR image of HP[^{13}C]bicarbonate in the anterior wall of the myocardium. The inhomogeneous [^{13}C]bicarbonate signal is due to the high local sensitivity of the surface coil. *Bottom panel*: Stacked plots showing the evolution of HP[^{13}C]bicarbonate and other metabolites in the myocardium after infusion of HP[1-^{13}C]bicarbonate. Eating a high-fat, high-sucrose Western diet (WD) was associated with suppression of HP[^{13}C]bicarbonate appearance, presumably due to increased oxidation of fatty acids. Data from Seymour et al. Cardiovasc Res. 2015; 106: 249-60

pioglitazone therapy does not have a significant effect on myocardial fatty acid metabolism [200]. The lack of a decrease in fatty acid metabolism and variable response in myocardial glucose uptake with these therapies may be explained by different responses in men and women. In men, metformin alone decreases whole-body fatty acid clearance, which results in increased plasma fatty acid levels, myocardial fatty acid uptake and oxidation, and lower myocardial glucose uptake. In women, myocardial glucose uptake is increased. When metformin and rosiglitazone are combined, women exhibit increased whole-body fatty acid clearance, which decreases plasma fatty acid levels and myocardial fatty acid uptake. This effect is much less pronounced in men. Group and sex also interacted in determining myocardial glucose uptake. Thus, in diabetes, different therapeutic regimens impact myocardial metabolism in a sex-specific manner. Of note for all of the studies above, metabolic response could not be predicted by changes in the plasma glucose or $HgBA1_C$ levels. Although requiring further evaluation in larger studies, these observations suggest metabolic imaging may be used to follow the effects of therapies designed to alter myocardial substrate metabolism in patients with diseases such as diabetes mellitus where more readily available clinical parameters are not

predictive of a therapeutic response. Moreover, they suggest more personalized approaches that incorporate patient gender may be useful in designing diabetic therapies.

HP MR

Compared to PET technology, there are limited examples of studies in vivo using HP-^{13}C to examine cardiac lipotoxicity in insulin resistance and diabetes mellitus. Nonetheless, early-stage investigations have begun to explore the metabolic consequences of diabetes and high fat diets. For example, it is known that malonyl-CoA is a critical regulator of fatty acid oxidation and the concentration of malonyl-CoA in diabetic myocardium is reduced. Since carnitine acetyltransferase is inhibited by malonyl-CoA, the rate of conversion of acetate to acetylcarnitine could be increased, potentially providing an important imaging biomarker of abnormal fatty acid oxidation. Metabolism of [1-^{13}C]acetate has been examined by hyperpolarization methods in perfused hearts and in vivo demonstrating the capacity to detect metabolism to [1-^{13}C]acetylcarnitine [101, 103, 153]. The effect of type 1 diabetes, modeled by administration of streptozotocin to rats, was examined using HP[1-^{13}C]acetate [202]. As outlined above, after activation by acetyl-CoA synthetase to acetyl-CoA, [1-^{13}C]acetate may be metabolized to [1-^{13}C]acetylcarnitine or [5-^{13}C]citrate. The focus of this study was on detection of [1-^{13}C]acetylcarnitine because the chemical shift difference between [5-^{13}C]citrate and [1-^{13}C]acetate is too small for resolution in vivo at clinical fields, although sufficient resolution is achievable in perfused hearts [102]. However, in spite of marked hyperglycemia after 3 weeks, induced by streptozotocin, there was no effect of type 1 diabetes on HP[1-^{13}C]acetylcarnitine/HP[1-^{13}C]acetate. Although further study is necessary to interpret this finding, these results may indicate that flux through the acetyl-CoA pool is small compared to the activity of an exchange reaction and that a reduction in activity of carnitine acetyltransferase is for this reason undetectable. These results were consistent with other exams detecting the products of [1-^{13}C]acetate metabolism: signal is modest compared to results from HP[1-^{13}C]pyruvate.

"Western" diets, modeled in rodents by high saturated lipid and sucrose content, are associated with insulin resistance and reduced left ventricular function [203–205]. In its early stages, exposure to an excess of dietary fat may result in lipotoxicity. High fat diets rapidly inhibit PDH flux [206], at least in part due to selective increase in the expression of pyruvate dehydrogenase kinase. This effect is very rapid and sustained, occurring within the first day on a diet, and implies that PDH flux will be sensitized to the inhibitory effects of fatty acids, presumably due to high [acetyl-CoA]/[CoA]. These observations predict that an imaging biomarker of PDH flux and conversion of HP[1-^{13}C]pyruvate to HP[^{13}C]bicarbonate will be inhibited. High-quality [^{13}C]bicarbonate images were achieved, and as anticipated, PDH flux was reduced [207]. This occurred in the absence of structural or functional deterioration, suggesting that HP methods may be a very sensitive indicator of early changes in metabolism due to diet.

Potential Synergies

As emphasized above, the heart must be capable of quickly managing major shifts in the demand for energy production as well as discontinuities in the hormonal and substrate environment. This adaptability has been termed "metabolic flexibility" which in the context of type 2 diabetes is equivalent to insulin resistance. There is little information about the evolution of metabolic inflexibility in the hearts of adolescents at risk for type 2 diabetes and cardiac lipotoxicity because studies with ionizing radiation are difficult to justify. There is a significant need for imaging technology enabling metabolic exams in children that can be used over time to assess baseline physiology as well as the response to interventions. Combined PET and ^{13}C-HP studies employing PET/MR may help this regard. Strategies are currently designed and evaluated to permit whole-body PET/MR imaging with very low injectable doses of ^{18}FDG and MR attenuation resulting in significantly reduced radiation exposure. As a consequence, the PET component of the PET/MR study could be used for both baseline metabolic measurements and identifying key organs

or specific regions of interest where glucose metabolism is altered. In the latter, more in-depth metabolic interrogation could be performed with ^{13}C-HP.

11.6 The Future: Validation and the Potential of Combined PET and ^{13}C-HP

By dint of the aforementioned discussion, the combining of capabilities of PET and HPMR to simultaneously measure both imaging readouts with PET/MR has the potential to open entirely new avenues of scientific discovery. For example, it would now be possible to cross-calibrate and cross-validate both imaging technologies. From HPMR perspective, metabolic measurements using various ^{13}C tracers can be compared with their PET ^{11}C radiotracer counterparts to determine impact of non-tracer doses of substrate on myocardial metabolism. Conversely, measurements of various components of myocardial metabolism measured with PET and compartmental modeling (e.g., oxidation and storage) can be referenced to the true metabolic fate of the exogenous substrate measured with HPMR. Most exciting is the potential use of the quantitative capabilities of PET to facilitate the HPMR quantification of substrate flux through metabolic pathways of interest. Such information is attainable from a PET-derived input function, an MR tissue response, and knowledge of the MR tracer blood concentration. Such information is critical for the accurate interpretation of HPMR-derived measurements of disease effects and dose response. Finally, it is conceivable that investigations using hyperpolarized compounds may actually enable further development of new PET agents and further encourage the development of PET/MR. Clearly, significant technical developments in probe development and image acquisition, analysis, and display are going to be required to move these examples from theory to practice.

Even with these major advances, translation to clinical application of these combined imaging approaches will require overcoming several challenges. The typical paradigm for developing new imaging tests has been used to perform the exam in patients with suspected or known disease and then to compare the results to a "gold standard" metric which may be an accepted exam or results from pathology [208]. These studies typically report sensitivity, specificity, or receiver operating characteristic (ROC) analysis. More recently, investigators and policy makers have recognized that the number of potential imaging approaches and probes is steadily increasing and recognizing appropriate use may be difficult. Questions of clinical utility are premature at this point in the development of hyperpolarization because the technology is still evolving rapidly and numerous refinements are anticipated in the next few years. Nevertheless investigators should consider that the technology will likely be evaluated based on three classes of data to support clinical translation: analytical validity, clinical validity, and clinical utility [209, 210]. Analytic validity means the reproducibility and reliability of a measurement. Does an HP image really measure what it claims? Can the measurement be performed reliably? Clinical validity refers to the relation between the imaging results and a clinical outcome or diagnosis of interest. Does an HP image detect clinically meaningful information, as judged by a reference standard? Very importantly, has HP imaging been tested against a technology with which clinicians are comfortable? Clinical utility is the most difficult challenge and tests whether the use of HP imaging results in a favorable redistribution of benefits compared to risks and costs. Does the use of HP imaging lead to improved outcomes, compared to nonuse? Eventually, these questions will need to be addressed, presumably through large multicenter prospective trials.

References

1. Ardenkjaer-Larsen JH, et al. Increase in signal-to-noise ratio of > 10,000 times in liquid-state NMR. Proc Natl Acad Sci U S A. 2003;100(18):10158–63.
2. Golman K, et al. Molecular imaging with endogenous substances. Proc Natl Acad Sci U S A. 2003;100(18):10435–9.
3. Nelson SJ, et al. Metabolic imaging of patients with prostate cancer using hyperpolarized [1-(1)(3)C] pyruvate. Sci Transl Med. 2013; 5(198): 198ra108.

4. Taegtmeyer H. Six blind men explore an elephant: aspects of fuel metabolism and the control of tricarboxylic acid cycle activity in heart muscle. Basic Res Cardiol. 1984;79(3):322–36.
5. Moreno KX, et al. Competition of pyruvate with physiological substrates for oxidation by the heart: implications for studies with hyperpolarized [1-13C]pyruvate. Am J Physiol Heart Circ Physiol. 2010;298(5):H1556–64.
6. Jeffrey FM, et al. Substrate selection in the isolated working rat heart: effects of reperfusion, afterload, and concentration. Basic Res Cardiol. 1995;90(5):388–96.
7. Jeffrey FM, et al. Direct evidence that perhexiline modifies myocardial substrate utilization from fatty acids to lactate. J Cardiovasc Pharmacol. 1995;25(3):469–72.
8. Drake AJ, Haines JR, Noble MI. Preferential uptake of lactate by the normal myocardium in dogs. Cardiovasc Res. 1980;14(2):65–72.
9. Banke NH, et al. Preferential oxidation of triacylglyceride-derived fatty acids in heart is augmented by the nuclear receptor PPARalpha. Circ Res. 2010;107(2):233–41.
10. Saddik M, Lopaschuk GD. Myocardial triglyceride turnover and contribution to energy substrate utilization in isolated working rat hearts. J Biol Chem. 1991;266(13):8162–70.
11. Armbrecht JJ, Buxton DB, Schelbert HR. Validation of [1-11C]acetate as a tracer for noninvasive assessment of oxidative metabolism with positron emission tomography in normal, ischemic, postischemic, and hyperemic canine myocardium. Circulation. 1990;81(5):1594–605.
12. Abbas AS, Wu G, Schulz H. Carnitine acetyltransferase is not a cytosolic enzyme in rat heart and therefore cannot function in the energy-linked regulation of cardiac fatty acid oxidation. J Mol Cell Cardiol. 1998;30(7):1305–9.
13. Bakker A, et al. Ultrastructural localisation of carnitine acetyltransferase activity in mitochondria of rat myocardium. Biochim Biophys Acta. 1994;1185(1):97–102.
14. Remesy C, Demigne C. Changes in availability of glucogenic and ketogenic substrates and liver metabolism in fed or starved rats. Ann Nutr Metab. 1983;27(1):57–70.
15. Owen OE, et al. Liver and kidney metabolism during prolonged starvation. J Clin Invest. 1969;48(3):574–83.
16. Hansford RG, Cohen L. Relative importance of pyruvate dehydrogenase interconversion and feedback inhibition in the effect of fatty acids on pyruvate oxidation by rat heart mitochondria. Arch Biochem Biophys. 1978;191(1):65–81.
17. Latipaa PM, et al. Regulation of pyruvate dehydrogenase during infusion of fatty acids of varying chain lengths in the perfused rat heart. J Mol Cell Cardiol. 1985;17(12):1161–71.
18. Purmal C, et al. Propionate stimulates pyruvate oxidation in the presence of acetate. Am J Physiol Heart Circ Physiol. 2014;307(8):H1134–41.
19. Bunger R. Compartmented pyruvate in perfused working heart. Am J Phys. 1985;249(3 Pt 2):H439–49.
20. Malloy CR, Sherry AD, Jeffrey FM. Evaluation of carbon flux and substrate selection through alternate pathways involving the citric acid cycle of the heart by 13C NMR spectroscopy. J Biol Chem. 1988;263(15):6964–71.
21. Peuhkurinen KJ, et al. Role of pyruvate carboxylation in the energy-linked regulation of pool sizes of tricarboxylic acid-cycle intermediates in the myocardium. Biochem J. 1982;208(3):577–81.
22. Depre C, Vanoverschelde JL, Taegtmeyer H. Glucose for the heart. Circulation. 1999;99(4):578–88.
23. Zimmer HG. Regulation of and intervention into the oxidative pentose phosphate pathway and adenine nucleotide metabolism in the heart. Mol Cell Biochem. 1996;160-161:101–9.
24. Zimmer HG. The oxidative pentose phosphate pathway in the heart: regulation, physiological significance, and clinical implications. Basic Res Cardiol. 1992;87(4):303–16.
25. Vimercati C, et al. Beneficial effects of acute inhibition of the oxidative pentose phosphate pathway in the failing heart. Am J Physiol Heart Circ Physiol. 2014;306(5):H709–17.
26. Nuutinen EM, et al. Elimination and replenishment of tricarboxylic acid-cycle intermediates in myocardium. Biochem J. 1981;194(3):867–75.
27. Peuhkurinen KJ, Hiltunen JK, Hassinen IE. Metabolic compartmentation of pyruvate in the isolated perfused rat heart. Biochem J. 1983;210(1):193–8.
28. Peuhkurinen KJ, Hassinen IE. Pyruvate carboxylation as an anaplerotic mechanism in the isolated perfused rat heart. Biochem J. 1982;202(1):67–76.
29. Sherry AD, et al. Propionate metabolism in the rat heart by 13C n.M.R. Spectroscopy. Biochem J. 1988;254(2):593–8.
30. Chatham JC, Forder JR. Metabolic compartmentation of lactate in the glucose-perfused rat heart. Am J Phys. 1996;270(1 Pt 2):H224–9.
31. Mowbray J, Ottaway JH. The flux of pyruvate in perfused rat heart. Eur J Biochem. 1973;36(2):362–8.
32. Mowbray J, Ottaway JH. The effect of insulin and growth hormone on the flux of tracer from labelled lactate in perfused rat heart. Eur J Biochem. 1973;36(2):369–79.
33. Li Q, et al. Multiple mass isotopomer tracing of acetyl-CoA metabolism in Langendorff-perfused rat hearts: channeling of acetyl-CoA from pyruvate dehydrogenase to carnitine acetyltransferase. J Biol Chem. 2015;290(13):8121–32.
34. Anousis N, et al. Compartmentation of glycolysis and glycogenolysis in the perfused rat heart. NMR Biomed. 2004;17(2):51–9.
35. Khemtong C, et al. Hyperpolarized 13C NMR detects rapid drug-induced changes in cardiac metabolism. Magn Reson Med. 2015;74(2):312–9.
36. Schinkel AF, et al. Hibernating myocardium: diagnosis and patient outcomes. Curr Probl Cardiol. 2007;32(7):375–410.

37. DeGrado TR, et al. Quantitative analysis of myocardial kinetics of 15-p-[iodine-125] iodophenylpentadecanoic acid. J Nucl Med. 1989;30(7):1211–8.
38. Dormehl IC, et al. Planar myocardial imaging in the baboon model with iodine-123-15-(iodophenyl) pentadecanoic acid (IPPA) and iodine-123-15-(P-iodophenyl)-3-R,S-methylpentadecanoic acid (BMIPP), using time-activity curves for evaluation of metabolism. Nucl Med Biol. 1995;22(7):837–47.
39. Eckelman WC, Babich JW. Synthesis and validation of fatty acid analogs radiolabeled by nonisotopic substitution. J Nucl Cardiol. 2007;14(3 Suppl):S100–9.
40. Ambrose KR, et al. Evaluation of the metabolism in rat hearts of two new radioiodinated 3-methyl-branched fatty acid myocardial imaging agents. Eur J Nucl Med. 1987;12(10):486–91.
41. Goodman MM, Kirsch G, Knapp FF Jr. Synthesis and evaluation of radioiodinated terminal p-iodophenyl-substituted alpha- and beta-methyl-branched fatty acids. J Med Chem. 1984;27(3):390–7.
42. Reske SN, et al. Metabolism of 15 (p 123I iodophenyl-)pentadecanoic acid in heart muscle and noncardiac tissues. Eur J Nucl Med. 1985;10(5-6):228–34.
43. He ZX, et al. Direct imaging of exercise-induced myocardial ischemia with fluorine-18-labeled deoxyglucose and Tc-99m-sestamibi in coronary artery disease. Circulation. 2003;108(10):1208–13.
44. Iida H, et al. Noninvasive quantification of regional myocardial metabolic rate for oxygen by use of 15O2 inhalation and positron emission tomography. Theory, error analysis, and application in humans. Circulation. 1996;94(4):792–807.
45. Laine H, et al. Myocardial oxygen consumption is unchanged but efficiency is reduced in patients with essential hypertension and left ventricular hypertrophy. Circulation. 1999;100(24):2425–30.
46. Yamamoto Y, et al. Noninvasive quantification of regional myocardial metabolic rate of oxygen by 15O2 inhalation and positron emission tomography, experimental validation. Circulation. 1996;94(4):808–16.
47. Brown M, et al. Delineation of myocardial oxygen utilization with carbon-11-labeled acetate. Circulation. 1987;76(3):687–96.
48. Brown MA, Myears DW, Bergmann SR. Noninvasive assessment of canine myocardial oxidative metabolism with carbon-11 acetate and positron emission tomography. J Am Coll Cardiol. 1988;12(4):1054–63.
49. Buck A, et al. Effect of carbon-11-acetate recirculation on estimates of myocardial oxygen consumption by PET. J Nucl Med. 1991;32(10):1950–7.
50. Sun KT, et al. Simultaneous measurement of myocardial oxygen consumption and blood flow using [1-carbon-11]acetate. J Nucl Med. 1998;39(2):272–80.
51. Choi Y, et al. Parametric images of myocardial metabolic rate of glucose generated from dynamic cardiac PET and 2-[18F]fluoro-2-deoxy-d-glucose studies. J Nucl Med. 1991;32(4):733–8.
52. Gambert S, et al. Adverse effects of free fatty acid associated with increased oxidative stress in post-ischemic isolated rat hearts. Mol Cell Biochem. 2006;283(1-2):147–52.
53. Iozzo P, et al. Regional myocardial blood flow and glucose utilization during fasting and physiological hyperinsulinemia in humans. Am J Physiol Endocrinol Metab. 2002;282(5):E1163–71.
54. Krivokapich J, et al. Fluorodeoxyglucose rate constants, lumped constant, and glucose metabolic rate in rabbit heart. Am J Phys. 1987;252(4 Pt 2):H777–87.
55. Botker HE, et al. Glucose uptake and lumped constant variability in normal human hearts determined with [18F]fluorodeoxyglucose. J Nucl Cardiol. 1997;4(2 Pt 1):125–32.
56. Hariharan R, et al. Fundamental limitations of [18F]2-deoxy-2-fluoro-D-glucose for assessing myocardial glucose uptake. Circulation. 1995;91(9):2435–44.
57. Hashimoto K, et al. Lumped constant for deoxyglucose is decreased when myocardial glucose uptake is enhanced. Am J Phys. 1999;276(1 Pt 2):H129–33.
58. Herrero P, et al. L-3-11C-lactate as a PET tracer of myocardial lactate metabolism: a feasibility study. J Nucl Med. 2007;48(12):2046–55.
59. Bergmann SR, et al. Quantitation of myocardial fatty acid metabolism using PET. J Nucl Med. 1996;37(10):1723–30.
60. Herrero P, et al. Increased myocardial fatty acid metabolism in patients with type 1 diabetes mellitus. J Am Coll Cardiol. 2006;47(3):598–604.
61. Kisrieva-Ware Z, et al. Assessment of myocardial triglyceride oxidation with PET and 11C-palmitate. J Nucl Cardiol.
62. DeGrado TR. Synthesis of 14(R,S)-[18F]fluoro-6-thia-heptadecanoic acid (FTHA). J Label Comp Radiopharm. 1991;29:989–95.
63. DeGrado TR, Coenen HH, Stocklin G. 14(R,S)-[18F]fluoro-6-thia-heptadecanoic acid (FTHA): evaluation in mouse of a new probe of myocardial utilization of long chain fatty acids. J Nucl Med. 1991;32(10):1888–96.
64. DeGrado TR, et al. Synthesis and preliminary evaluation of (18)F-labeled 4-thia palmitate as a PET tracer of myocardial fatty acid oxidation. Nucl Med Biol. 2000;27(3):221–31.
65. DeGrado TR, et al. Validation of 18F-fluoro-4-thia-palmitate as a PET probe for myocardial fatty acid oxidation: effects of hypoxia and composition of exogenous fatty acids. J Nucl Med. 2006;47(1):173–81.
66. DeGrado TR, et al. Synthesis and preliminary evaluation of 18-(18)F-fluoro-4-thia-oleate as a PET probe of fatty acid oxidation. J Nucl Med. 2010;51(8):1310–7.
67. Shoup TM, et al. Evaluation of trans-9-18F-fluoro-3,4-Methyleneheptadecanoic acid as a PET tracer for myocardial fatty acid imaging. J Nucl Med. 2005;46(2):297–304.

68. Demeure F, et al. A new F-18 labeled PET tracer for fatty acid imaging. J Nucl Cardiol. 2015;22(2):391–4.
69. Labbe SM, et al. Increased myocardial uptake of dietary fatty acids linked to cardiac dysfunction in glucose-intolerant humans. Diabetes. 2012;61(11):2701–10.
70. Labbe SM, et al. Organ-specific dietary fatty acid uptake in humans using positron emission tomography coupled to computed tomography. Am J Physiol Endocrinol Metab. 2011;300(3):E445–53.
71. Shoghi KI, Gropler RJ. PET measurements of organ metabolism: the devil is in the details. Diabetes. 2015;64(7):2332–4.
72. O'Donnell JM, et al. The absence of endogenous lipid oxidation in early stage heart failure exposes limits in lipid storage and turnover. J Mol Cell Cardiol. 2008;44(2):315–22.
73. Saddik M, Lopaschuk GD. Triacylglycerol turnover in isolated working hearts of acutely diabetic rats. Can J Physiol Pharmacol. 1994;72(10):1110–9.
74. Wisneski JA, et al. Myocardial metabolism of free fatty acids. Studies with 14C-labeled substrates in humans. J Clin Invest. 1987;79(2):359–66.
75. Wicklmayr M, et al. Inhibition of muscular triglyceride lipolysis by ketone bodies: a mechanism for energy-preservation in starvation. Horm Metab Res. 1986;18(7):476–8.
76. Kisrieva-Ware Z, et al. Assessment of myocardial triglyceride oxidation with PET and 11C-palmitate. J Nucl Cardiol. 2009;16(3):411–21.
77. Bucci M, et al. Trimetazidine reduces endogenous free fatty acid oxidation and improves myocardial efficiency in obese humans. Cardiovasc Ther. 2012;30(6):333–41.
78. Brindle KM. Imaging metabolism with hyperpolarized (13)C-labeled cell substrates. J Am Chem Soc. 2015;137(20):6418–27.
79. Comment A, Merritt ME. Hyperpolarized magnetic resonance as a sensitive detector of metabolic function. Biochemistry. 2014;53(47):7333–57.
80. Kurhanewicz J, et al. Analysis of cancer metabolism by imaging hyperpolarized nuclei: prospects for translation to clinical research. Neoplasia. 2011;13(2):81–97.
81. Bhattacharya P, Ross BD, Bunger R. Cardiovascular applications of hyperpolarized contrast media and metabolic tracers. Exp Biol Med (Maywood). 2009;234(12):1395–416.
82. Tyler DJ. Cardiovascular applications of hyperpolarized MRI. Curr Cardiovasc Imaging Rep. 2011;4(2):108–15.
83. Rider OJ, Tyler DJ. Clinical implications of cardiac hyperpolarized magnetic resonance imaging. J Cardiovasc Magn Reson. 2013;15:93.
84. Keshari KR, Wilson DM. Chemistry and biochemistry of 13C hyperpolarized magnetic resonance using dynamic nuclear polarization. Chem Soc Rev. 2014;43(5):1627–59.
85. Lau AZ, et al. Simultaneous assessment of cardiac metabolism and perfusion using copolarized [1-13 C]pyruvate and 13 C-urea. Magn Reson Med. 2016.
86. Golman K, Petersson JS. Metabolic imaging and other applications of hyperpolarized 13C1. Acad Radiol. 2006;13(8):932–42.
87. Golman K, et al. Cardiac metabolism measured noninvasively by hyperpolarized 13C MRI. Magn Reson Med. 2008;59(5):1005–13.
88. Lau AZ, et al. Rapid multislice imaging of hyperpolarized 13C pyruvate and bicarbonate in the heart. Magn Reson Med. 2010;64(5):1323–31.
89. Schroeder MA, et al. Hyperpolarized (13)C magnetic resonance reveals early- and late-onset changes to in vivo pyruvate metabolism in the failing heart. Eur J Heart Fail. 2013;15(2):130–40.
90. Merritt ME, et al. Hyperpolarized 13C allows a direct measure of flux through a single enzyme-catalyzed step by NMR. Proc Natl Acad Sci U S A. 2007;104(50):19773–7.
91. Lau, A.Z., J.J. Miller, and D.J. Tyler, Mapping of intracellular pH in the in vivo rodent heart using hyperpolarized [1-13C]pyruvate. Magn Reson Med, 2016.
92. Dominguez-Viqueira W, et al. Intensity correction for multichannel hyperpolarized 13C imaging of the heart. Magn Reson Med. 2016;75(2):859–65.
93. Schroeder MA, et al. Real-time assessment of Krebs cycle metabolism using hyperpolarized 13C magnetic resonance spectroscopy. FASEB J. 2009;23(8):2529–38.
94. Chen AP, et al. Simultaneous investigation of cardiac pyruvate dehydrogenase flux, Krebs cycle metabolism and pH, using hyperpolarized [1,2-(13)C2] pyruvate in vivo. NMR Biomed. 2012;25(2):305–11.
95. Chen AP, et al. Using [1-(13) C]lactic acid for hyperpolarized (13) C MR cardiac studies. Magn Reson Med. 2015;73(6):2087–93.
96. Jensen PR, et al. Tissue-specific short chain fatty acid metabolism and slow metabolic recovery after ischemia from hyperpolarized NMR in vivo. J Biol Chem. 2009;284(52):36077–82.
97. Bastiaansen JA, et al. Direct noninvasive estimation of myocardial tricarboxylic acid cycle flux in vivo using hyperpolarized (1)(3)C magnetic resonance. J Mol Cell Cardiol. 2015;87:129–37.
98. Flori A, et al. Real-time cardiac metabolism assessed with hyperpolarized [1-(13) C]acetate in a large-animal model. Contrast Media Mol Imaging. 2015;10(3):194–202.
99. Ball DR, et al. Hyperpolarized butyrate: a metabolic probe of short chain fatty acid metabolism in the heart. Magn Reson Med. 2014;71(5):1663–9.
100. Vary TC, Reibel DK, Neely JR. Control of energy metabolism of heart muscle. Annu Rev Physiol. 1981;43:419–30.
101. Neely JR, Morgan HE. Relationship between carbohydrate and lipid metabolism and the energy balance of heart muscle. Annu Rev Physiol. 1974;36:413–59.
102. Lopaschuk G. Regulation of carbohydrate metabolism in ischemia and reperfusion. Am Heart J. 2000;139(2 Pt 3):S115–9.
103. Araujo LI, et al. Abnormalities in myocardial metabolism in patients with unstable angina as assessed

by positron emission tomography. Cardiovasc Drugs Ther. 1988;2(1):41–6.
104. Camici P, et al. Increased uptake of 18F-fluorodeoxyglucose in postischemic myocardium of patients with exercise-induced angina. Circulation. 1986;74(1):81–8.
105. Tamaki N, et al. The role of fatty acids in cardiac imaging. J Nucl Med. 2000;41(9):1525–34.
106. Kawai Y, et al. Diagnostic value of 123I-betamethyl-p-iodophenyl-pentadecanoic acid (BMIPP) single photon emission computed tomography (SPECT) in patients with chest pain. Comparison with rest-stress 99mTc-tetrofosmin SPECT and coronary angiography. Circ J. 2004;68(6):547–52.
107. Kontos MC, et al. Iodofiltic acid I 123 (BMIPP) fatty acid imaging improves initial diagnosis in emergency department patients with suspected acute coronary syndromes: a multicenter trial. J Am Coll Cardiol. 2010;56(4):290–9.
108. Moroi M, et al. Association between abnormal myocardial fatty acid metabolism and cardiac-derived death among patients undergoing hemodialysis: results from a cohort study in Japan. Am J Kidney Dis. 2013;61(3):466–75.
109. Dou KF, et al. Myocardial 18F-FDG uptake after exercise-induced myocardial ischemia in patients with coronary artery disease. J Nucl Med. 2008;49(12):1986–91.
110. Merritt ME, et al. Inhibition of carbohydrate oxidation during the first minute of reperfusion after brief ischemia: NMR detection of hyperpolarized 13CO2 and H13CO3. Magn Reson Med. 2008;60(5):1029–36.
111. Rupp H, Jacob R. Metabolically-modulated growth and phenotype of the rat heart. Eur Heart J. 1992;13(Suppl D):56–61.
112. Barger PM, Kelly DP. Fatty acid utilization in the hypertrophied and failing heart: molecular regulatory mechanisms. Am J Med Sci. 1999;318(1):36–42.
113. Tuder RM, Davis LA, Graham BB. Targeting energetic metabolism: a new frontier in the pathogenesis and treatment of pulmonary hypertension. Am J Respir Crit Care Med. 2012;185(3):260–6.
114. Kolwicz SC Jr. And R. Tian, glucose metabolism and cardiac hypertrophy. Cardiovasc Res. 2011;90(2):194–201.
115. Taegtmeyer H, et al. Linking gene expression to function: metabolic flexibility in the normal and diseased heart. Ann N Y Acad Sci. 2004;1015:202–13.
116. Jamshidi Y, et al. Peroxisome proliferator-activated receptor alpha gene regulates left ventricular growth in response to exercise and hypertension. Circulation. 2002;105(8):950–5.
117. Blair E, et al. Mutations in the gamma(2) subunit of AMP-activated protein kinase cause familial hypertrophic cardiomyopathy: evidence for the central role of energy compromise in disease pathogenesis. Hum Mol Genet. 2001;10(11):1215–20.
118. Razeghi P, et al. Downregulation of myocardial myocyte enhancer factor 2C and myocyte enhancer factor 2C-regulated gene expression in diabetic patients with nonischemic heart failure. Circulation. 2002;106(4):407–11.
119. Buttrick PM, et al. Alterations in gene expression in the rat heart after chronic pathological and physiological loads. J Mol Cell Cardiol. 1994;26(1):61–7.
120. Ouwens DM, et al. Cardiac contractile dysfunction in insulin-resistant rats fed a high-fat diet is associated with elevated CD36-mediated fatty acid uptake and esterification. Diabetologia. 2007;50(9):1938–48.
121. Handa N, et al. Quantitative FDG-uptake by positron emission tomography in progressive hypertrophy of rat hearts in vivo. Ann Nucl Med. 2007;21(10):569–76.
122. Banke NH, et al. Sexual dimorphism in cardiac triacylglyceride dynamics in mice on long term caloric restriction. J Mol Cell Cardiol. 2012;52(3):733–40.
123. Hollingsworth KG, et al. Left ventricular torsion, energetics, and diastolic function in normal human aging. Am J Physiol Heart Circ Physiol. 2012;302(4):H885–92.
124. van der Meer RW, et al. The ageing male heart: myocardial triglyceride content as independent predictor of diastolic function. Eur Heart J. 2008;29(12):1516–22.
125. Zhong M, et al. Quantitative PET imaging detects early metabolic remodeling in a mouse model of pressure-overload left ventricular hypertrophy in vivo. J Nucl Med. 2013;54(4):609–15.
126. de las Fuentes L, et al. Myocardial fatty acid metabolism: independent predictor of left ventricular mass in hypertensive heart disease. Hypertension. 2003; 41(1): 83–7.
127. Hamirani YS, et al. Noninvasive detection of early metabolic left ventricular remodeling in systemic hypertension. Cardiology. 2016;133(3):157–62.
128. Lundgrin EL, et al. Fasting 2-deoxy-2-[18F]fluoro-D-glucose positron emission tomography to detect metabolic changes in pulmonary arterial hypertension hearts over 1 year. Ann Am Thorac Soc. 2013;10(1):1–9.
129. Bokhari S, et al. PET imaging may provide a novel biomarker and understanding of right ventricular dysfunction in patients with idiopathic pulmonary arterial hypertension. Circ Cardiovasc Imaging. 2011;4(6):641–7.
130. Fang W, et al. Comparison of 18F-FDG uptake by right ventricular myocardium in idiopathic pulmonary arterial hypertension and pulmonary arterial hypertension associated with congenital heart disease. Pulm Circ. 2012;2(3):365–72.
131. Tatebe S, et al. Enhanced [18F]fluorodeoxyglucose accumulation in the right ventricular free wall predicts long-term prognosis of patients with pulmonary hypertension: a preliminary obser-

vational study. Eur Heart J Cardiovasc Imaging. 2014;15(6):666–72.
132. Oikawa M, et al. Increased [18F]fluorodeoxyglucose accumulation in right ventricular free wall in patients with pulmonary hypertension and the effect of epoprostenol. J Am Coll Cardiol. 2005;45(11):1849–55.
133. Mielniczuk LM, et al. Relation between right ventricular function and increased right ventricular [18F]fluorodeoxyglucose accumulation in patients with heart failure. Circ Cardiovasc Imaging. 2011;4(1):59–66.
134. Nakae I, et al. Iodine-123 BMIPP scintigraphy in the evaluation of patients with heart failure. Acta Radiol. 2006;47(8):810–6.
135. Davila-Roman VG, et al. Altered myocardial fatty acid and glucose metabolism in idiopathic dilated cardiomyopathy. J Am Coll Cardiol. 2002;40(2):271–7.
136. Kadkhodayan, A., et al., Sex affects myocardial blood flow and fatty acid substrate metabolism in humans with nonischemic heart failure. J Nucl Cardiol, 2016.
137. Tuunanen H, et al. Decreased myocardial free fatty acid uptake in patients with idiopathic dilated cardiomyopathy: evidence of relationship with insulin resistance and left ventricular dysfunction. J Card Fail. 2006;12(8):644–52.
138. Sharma S, et al. Intramyocardial lipid accumulation in the failing human heart resembles the lipotoxic rat heart. FASEB J. 2004;18(14):1692–700.
139. Thackery J, dR, Beanlands R, DaSilva J. Early diabetes therapy does not prevent sympathetic dysinnervation in the streptozocin diabetic rat. J Nucl Cardiol. 2014.
140. Vinik AI, Maser RE, Ziegler D. Neuropathy: the crystal ball for cardiovascular disease? Diabetes Care. 2010;33(7):1688–90.
141. Boulton AJ, et al. Diabetic neuropathies: a statement by the American Diabetes Association. Diabetes Care. 2005;28(4):956–62.
142. Tuunanen H, et al. Trimetazidine, a metabolic modulator, has cardiac and extracardiac benefits in idiopathic dilated cardiomyopathy. Circulation. 2008;118(12):1250–8.
143. Lepore, J.J., et al., Effects of the novel long-acting GLP-1 agonist, Albiglutide, on cardiac function, cardiac metabolism, and exercise capacity in patients with chronic heart failure and reduced ejection fraction. JACC Heart Fail, 2016.
144. Atherton HJ, et al. Role of pyruvate dehydrogenase inhibition in the development of hypertrophy in the hyperthyroid rat heart: a combined magnetic resonance imaging and hyperpolarized magnetic resonance spectroscopy study. Circulation. 2011;123(22):2552–61.
145. Brown MA, Myears DW, Bergmann SR. Validity of estimates of myocardial oxidative metabolism with carbon-11 acetate and positron emission tomography despite altered patterns of substrate utilization. J Nucl Med. 1989;30(2):187–93.
146. Walsh MN, et al. Noninvasive estimation of regional myocardial oxygen consumption by positron emission tomography with carbon-11 acetate in patients with myocardial infarction. J Nucl Med. 1989;30(11):1798–808.
147. Buxton DB, et al. Radiolabeled acetate as a tracer of myocardial tricarboxylic acid cycle flux. Circ Res. 1988;63(3):628–34.
148. Koellisch U, et al. Metabolic imaging of hyperpolarized [1-(13) C]acetate and [1-(13) C]acetylcarnitine - investigation of the influence of dobutamine induced stress. Magn Reson Med. 2015;74(4):1011–8.
149. Bastiaansen JA, Merritt ME, Comment A. Measuring changes in substrate utilization in the myocardium in response to fasting using hyperpolarized [1-(13)C] butyrate and [1-(13)C]pyruvate. Sci Rep. 2016;6:25573.
150. Erguven M, et al. A case of early diagnosed carnitine deficiency presenting with respiratory symptoms. Ann Nutr Metab. 2007;51(4):331–4.
151. Rinaldo P, Matern D, Bennett MJ. Fatty acid oxidation disorders. Annu Rev Physiol. 2002;64:477–502.
152. Palmieri F. Diseases caused by defects of mitochondrial carriers: a review. Biochim Biophys Acta. 2008;1777(7-8):564–78.
153. Cave MC, et al. Obesity, inflammation, and the potential application of pharmaconutrition. Nutr Clin Pract. 2008;23(1):16–34.
154. Kenchaiah S, et al. Obesity and the risk of heart failure. N Engl J Med. 2002;347(5):305–13.
155. Wong CY, et al. Alterations of left ventricular myocardial characteristics associated with obesity. Circulation. 2004;110(19):3081–7.
156. Zhou YT, et al. Lipotoxic heart disease in obese rats: implications for human obesity. Proc Natl Acad Sci U S A. 2000;97(4):1784–9.
157. Commerford SR, et al. Fat oxidation, lipolysis, and free fatty acid cycling in obesity-prone and obesity-resistant rats. Am J Physiol Endocrinol Metab. 2000;279(4):E875–85.
158. Boudina S, Abel ED. Diabetic cardiomyopathy revisited. Circulation. 2007;115(25): 3213–23.
159. Severson DL. Diabetic cardiomyopathy: recent evidence from mouse models of type 1 and type 2 diabetes. Can J Physiol Pharmacol. 2004;82(10): 813–23.
160. Stanley WC, Lopaschuk GD, McCormack JG. Regulation of energy substrate metabolism in the diabetic heart. Cardiovasc Res. 1997;34(1):25–33.
161. Taegtmeyer H, McNulty P, Young ME. Adaptation and maladaptation of the heart in diabetes: part I: general concepts. Circulation. 2002;105(14):1727–33.
162. Young ME, McNulty P, Taegtmeyer H. Adaptation and maladaptation of the heart in diabetes: part II: potential mechanisms. Circulation. 2002;105(15):1861–70.
163. Itani SI, et al. Involvement of protein kinase C in human skeletal muscle insulin resistance and obesity. Diabetes. 2000;49(8):1353–8.

164. Ruderman NB, et al. Malonyl-CoA, fuel sensing, and insulin resistance. Am J Phys. 1999;276(1 Pt 1):E1–E18.
165. Schmitz-Peiffer C, Craig DL, Biden TJ. Ceramide generation is sufficient to account for the inhibition of the insulin-stimulated PKB pathway in C2C12 skeletal muscle cells pretreated with palmitate. J Biol Chem. 1999;274(34):24202–10.
166. Oakes ND, et al. Cardiac metabolism in mice: tracer method developments and in vivo application revealing profound metabolic inflexibility in diabetes. Am J Physiol Endocrinol Metab. 2006;290(5):E870–81.
167. Young ME, et al. Impaired long-chain fatty acid oxidation and contractile dysfunction in the obese Zucker rat heart. Diabetes. 2002;51(8):2587–95.
168. Peterson LR, et al. Effect of obesity and insulin resistance on myocardial substrate metabolism and efficiency in young women. Circulation. 2004;109(18):2191–6.
169. Buchanan J, et al. Reduced cardiac efficiency and altered substrate metabolism precedes the onset of hyperglycemia and contractile dysfunction in two mouse models of insulin resistance and obesity. Endocrinology. 2005;146(12):5341–9.
170. Mazumder PK, et al. Impaired cardiac efficiency and increased fatty acid oxidation in insulin-resistant ob/ob mouse hearts. Diabetes. 2004;53(9):2366–74.
171. Boudina S, Abel ED. Mitochondrial uncoupling: a key contributor to reduced cardiac efficiency in diabetes. Physiology (Bethesda). 2006;21:250–8.
172. Boudina S, et al. Reduced mitochondrial oxidative capacity and increased mitochondrial uncoupling impair myocardial energetics in obesity. Circulation. 2005;112(17):2686–95.
173. How OJ, et al. Increased myocardial oxygen consumption reduces cardiac efficiency in diabetic mice. Diabetes. 2006;55(2):466–73.
174. Peterson LR, et al. Impact of gender on the myocardial metabolic response to obesity. J Am Coll Cardiol Imaging. 2008;1:424–33.
175. Peterson LR, et al. Type 2 diabetes, obesity, and sex difference affect the fate of glucose in the human heart. Am J Physiol Heart Circ Physiol. 2015;308(12):H1510–6.
176. Viljanen AP, et al. Effect of caloric restriction on myocardial fatty acid uptake, left ventricular mass, and cardiac work in obese adults. Am J Cardiol. 2009;103(12):1721–6.
177. Lin CH, et al. Myocardial oxygen consumption change predicts left ventricular relaxation improvement in obese humans after weight loss. Obesity (Silver Spring). 2011;19(9):1804–12.
178. Finck BN, et al. The cardiac phenotype induced by PPARalpha overexpression mimics that caused by diabetes mellitus. J Clin Invest. 2002;109(1):121–30.
179. Burkart EM, et al. Nuclear receptors PPARbeta/delta and PPARalpha direct distinct metabolic regulatory programs in the mouse heart. J Clin Invest. 2007;117(12):3930–9.
180. Shoghi KI, et al. Time course of alterations in myocardial glucose utilization in the Zucker diabetic fatty rat with correlation to gene expression of glucose transporters: a small-animal PET investigation. J Nucl Med. 2008;49(8):1320–7.
181. van den Brom CE, et al. Altered myocardial substrate metabolism is associated with myocardial dysfunction in early diabetic cardiomyopathy in rats: studies using positron emission tomography. Cardiovasc Diabetol. 2009;8:39.
182. Thorn SL, et al. Repeatable noninvasive measurement of mouse myocardial glucose uptake with 18F-FDG: evaluation of tracer kinetics in a type 1 diabetes model. J Nucl Med. 2013;54(9):1637–44.
183. Herrero P, et al. PET detection of the impact of dobutamine on myocardial glucose metabolism in women with type 1 diabetes mellitus. J Nucl Cardiol. 2008;15(6):791–9.
184. Peterson LR, et al. Fatty acids and insulin modulate myocardial substrate metabolism in humans with type 1 diabetes. Diabetes. 2008;57(1):32–40.
185. Rijzewijk LJ, et al. Altered myocardial substrate metabolism and decreased diastolic function in nonischemic human diabetic cardiomyopathy: studies with cardiac positron emission tomography and magnetic resonance imaging. J Am Coll Cardiol. 2009;54(16):1524–32.
186. Peterson LR, et al. Sex and type 2 diabetes: obesity-independent effects on left ventricular substrate metabolism and relaxation in humans. Obesity (Silver Spring). 2012;20(4):802–10.
187. Monti LD, et al. Myocardial insulin resistance associated with chronic hypertriglyceridemia and increased FFA levels in type 2 diabetic patients. Am J Physiol Heart Circ Physiol. 2004;287(3):H1225–31.
188. McGill JB, et al. Potentiation of abnormalities in myocardial metabolism with the development of diabetes in women with obesity and insulin resistance. J Nucl Cardiol. 2011;18(3):421–9. quiz 432-3
189. Rijzewijk LJ, et al. Myocardial steatosis is an independent predictor of diastolic dysfunction in type 2 diabetes mellitus. J Am Coll Cardiol. 2008;52(22):1793–9.
190. Rijzewijk LJ, et al. Effects of hepatic triglyceride content on myocardial metabolism in type 2 diabetes. J Am Coll Cardiol. 2010;56(3):225–33.
191. Ng AC, et al. Myocardial steatosis and biventricular strain and strain rate imaging in patients with type 2 diabetes mellitus. Circulation. 2010;122(24):2538–44.
192. MacDonald MR, et al. Discordant short- and long-term outcomes associated with diabetes in patients with heart failure: importance of age and sex: a population study of 5.1 million people in Scotland. Circ Heart Fail. 2008;1(4):234–41.
193. Ho KK, et al. The epidemiology of heart failure: the Framingham study. J Am Coll Cardiol. 1993;22(4 Suppl A):6A–13A.
194. Gu K, Cowie CC, Harris MI. Diabetes and decline in heart disease mortality in US adults. JAMA. 1999;281(14):1291–7.

195. van der Meer RW, et al. Pioglitazone improves cardiac function and alters myocardial substrate metabolism without affecting cardiac triglyceride accumulation and high-energy phosphate metabolism in patients with well-controlled type 2 diabetes mellitus. Circulation. 2009;119(15):2069–77.
196. Hallsten K, et al. Enhancement of insulin-stimulated myocardial glucose uptake in patients with type 2 diabetes treated with rosiglitazone. Diabet Med. 2004;21(12):1280–7.
197. Koellisch U, et al. Investigation of metabolic changes in STZ-induced diabetic rats with hyperpolarized [1-13C]acetate. Physiol Rep. 2015;3(8):e12474.
198. Wilson CR, et al. Western diet, but not high fat diet, causes derangements of fatty acid metabolism and contractile dysfunction in the heart of Wistar rats. Biochem J. 2007;406(3):457–67.
199. Qin F, et al. The polyphenols resveratrol and S17834 prevent the structural and functional sequelae of diet-induced metabolic heart disease in mice. Circulation. 2012;125(14):1757–64. S1-6
200. Vasanji Z, et al. Alterations in cardiac contractile performance and sarcoplasmic reticulum function in sucrose-fed rats is associated with insulin resistance. Am J Physiol Cell Physiol. 2006;291(4):C772–80.
201. Crewe C, Kinter M, Szweda LI. Rapid inhibition of pyruvate dehydrogenase: an initiating event in high dietary fat-induced loss of metabolic flexibility in the heart. PLoS One. 2013;8(10):e77280.
202. Seymour AM, et al. In vivo assessment of cardiac metabolism and function in the abdominal aortic banding model of compensated cardiac hypertrophy. Cardiovasc Res. 2015;106(2):249–60.
203. Mankoff DA, et al. Molecular imaging research in the outcomes era: measuring outcomes for individualized cancer therapy. Acad Radiol. 2007;14(4):398–405.
204. McShane LM, Hayes DF. Publication of tumor marker research results: the necessity for complete and transparent reporting. J Clin Oncol. 2012;30(34):4223–32.
205. Henry NL, Hayes DF. Cancer biomarkers. Mol Oncol. 2012;6(2):140–6.